Quarterly Journal of the Royal Meteorological Society Q. J. R. Meteorol. Soc. 140: 2401–2419, October 2014 B DOI:10.1002/qj.2330

RMetS
Royal Meteorological Society

Review Article
Climate system response to stratospheric ozone depletion and recovery

Michael Previdi[a]* and Lorenzo M. Polvani[a,b]

[a]*Lamont-Doherty Earth Observatory of Columbia University, Palisades, NY, USA*
[b]*Department of Applied Physics and Applied Mathematics and Department of Earth and Environmental Sciences, Columbia University, New York, NY, USA*

*Correspondence to: M. Previdi, Lamont-Doherty Earth Observatory of Columbia University, 61 Route 9W, Palisades, NY 10964, USA.
E-mail: mprevidi@ldeo.columbia.edu

We review what is presently known about the climate system response to stratospheric ozone depletion and its projected recovery, focusing on the responses of the atmosphere, ocean and cryosphere. Compared with well-mixed greenhouse gases (GHGs), the radiative forcing of climate due to observed stratospheric ozone loss is very small: in spite of this, recent trends in stratospheric ozone have caused profound changes in the Southern Hemisphere (SH) climate system, primarily by altering the tropospheric midlatitude jet, which is commonly described as a change in the Southern Annular Mode. Ozone depletion in the late twentieth century was the primary driver of the observed poleward shift of the jet during summer, which has been linked to changes in tropospheric and surface temperatures, clouds and cloud radiative effects, and precipitation at both middle and low latitudes. It is emphasized, however, that not all aspects of the SH climate response to stratospheric ozone forcing can be understood in terms of changes in the midlatitude jet. The response of the Southern Ocean and sea ice to ozone depletion is currently a matter of debate. For the former, the debate is centred on the role of ocean eddies in possibly opposing wind-driven changes in the mean circulation. For the latter, the issue is reconciling the observed expansion of Antarctic sea-ice extent during the satellite era with robust modelling evidence that the ice should melt as a result of stratospheric ozone depletion (and increases in GHGs). Despite lingering uncertainties, it has become clear that ozone depletion has been instrumental in driving SH climate change in recent decades. Similarly, ozone recovery will figure prominently in future climate change, with its impacts expected to largely cancel the impacts of increasing GHGs during the next half-century.

Key Words: stratospheric ozone; climate change; Southern Annular Mode

Received 11 October 2013; Revised 20 December 2013; Accepted 6 January 2014; Published online in Wiley Online Library 25 March 2014

1. Introduction

Stratospheric ozone depletion due to human activity is one of the great environmental issues of the twentieth century. Global total column ozone amounts (which are dominated by ozone in the stratosphere) declined by a few per cent between roughly the 1970s and the start of the current century (WMO, 2011). However, this pales in comparison to the ozone depletion that was observed during the same period over Antarctica, where about half the total column ozone was lost during austral spring. The spatial scale of Antarctic ozone loss is immense, covering nearly the entire continent (Figure 1), and thus this phenomenon has been popularly christened the ozone 'hole'.

Stratospheric ozone depletion is now understood to be a consequence of anthropogenic emissions of trace gases, primarily chlorofluorocarbons (CFCs), but also other halogenated species containing chlorine and bromine. These gases are long lived in the atmosphere, and thus well mixed. In the stratosphere in the presence of solar ultraviolet (UV) radiation, they participate in catalytic chemical reactions that destroy ozone; see Solomon (1999) for a comprehensive review. Ozone loss is greatly accelerated in the Antarctic lower stratosphere (∼12 to 25 km altitude) during austral spring as a result of heterogeneous reactions occurring on the surfaces of polar stratospheric clouds (PSCs). These reactions serve to make the anthropogenic chlorine loading much more effective at destroying ozone, because a larger

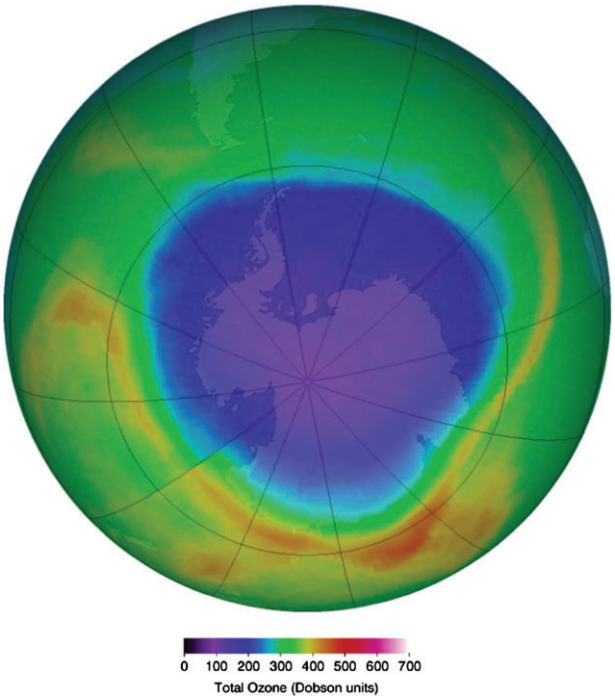

Figure 1. Satellite image from 4 October 2004, providing a representative illustration of the Antarctic ozone hole and its size in relation to the continent (courtesy of NASA; http://ozonewatch.gsfc.nasa.gov/Scripts/big_image.php?date=2004-10-04&hem=S).

fraction of the added chlorine is converted into active (i.e. ozone depleting) forms.

The discovery of the Antarctic ozone hole (Farman *et al.*, 1985), and subsequent understanding of its causes (Solomon *et al.*, 1986; Molina and Molina, 1987), led shortly thereafter to the ratification of the 1987 Montreal Protocol on Substances that Deplete the Ozone Layer. The Montreal Protocol is an international treaty that was designed to protect the ozone layer by phasing out the production of CFCs and other ozone depleting substances (ODSs). It grew out of concerns that the depletion of stratospheric ozone would lead to increased levels of UV radiation at the surface (because ozone absorbs in the UV portion of the spectrum), which would potentially have adverse effects on human health, agriculture and natural ecosystems. What was not appreciated at the time, however, and indeed not until very recently, are the significant and widespread climate effects associated with the development of the Antarctic ozone hole (e.g. see Thompson *et al.*, 2011). These climate effects are the subject of this review. As will be discussed, the climate impacts of the ozone hole extend from the stratosphere down to the surface, and from the Antarctic region throughout most of the Southern Hemisphere (SH).

The remainder of this article is organized as follows. Sections 2–4 consider the responses of different components of the climate system, specifically the atmosphere (section 2), ocean (section 3) and cryosphere (section 4), to stratospheric ozone depletion at the end of the twentieth century. In section 5, these responses to ozone depletion are contrasted with the expected responses to ozone recovery during the next several decades. Finally, in section 6, a summary and outlook are presented.

2. Atmospheric response to stratospheric ozone depletion

2.1. Observed stratospheric ozone and temperature changes

We start by recalling the remarkable loss of stratospheric ozone that was observed in the late twentieth century over Antarctica, illustrated in Figure 2. Ozone depletion of more than 80% is shown to occur in October in the lower stratosphere between roughly 60 and 100 hPa, and Figure 2 demonstrates the pronounced vertical structure and seasonality of the observed ozone losses. The losses are confined almost exclusively to the stratosphere (i.e. above ∼300 hPa), and to the austral spring season. As will be discussed below, this seasonal cycle of ozone depletion is key to establishing the prominent role of ozone forcing in producing many of the observed SH climate changes in recent decades.

The confinement to essentially a single season is one of several ways in which stratospheric ozone forcing differs from that due to anthropogenic well-mixed greenhouse gases (GHGs; e.g. CO_2, CH_4 and N_2O). Table 1 identifies some other notable differences between the two forcing agents. It is useful to briefly consider these differences, because they can provide information on the relative importance of stratospheric ozone and GHG trends in driving observed and model-simulated climate change. Stratospheric ozone forcing, in addition to having a strong seasonal dependence, also has a strong geographical dependence, with severe ozone depletion (i.e. the ozone hole) being restricted to the SH polar region (see Figure 1). This is in stark contrast to GHG forcing, which is significant globally. As will become clear in the discussion that follows, although the ozone hole itself is geographically localized its associated climate impacts are not, because they extend over the entire SH. Stratospheric ozone and GHG forcings also have very different time histories during the twentieth and twenty-first centuries. The GHG forcing increases monotonically over this entire period. In contrast, stratospheric ozone forcing starts to become significant only in the 1970s, and changes sign around the year 2000 as ozone depletion transitions to ozone recovery (in response to reduced anthropogenic halogen loading). Finally, the magnitude of the global annual mean radiative forcing due to increasing GHGs is substantially greater than that due to stratospheric ozone depletion. The former is the largest anthropogenic forcing, with an estimated magnitude (in 2005 relative to pre-industrial) of 2.6 W m^{-2} (Forster *et al.*, 2007). In contrast, the global mean stratospheric ozone forcing is not even significantly different from zero at the 90% confidence level (Table 1). This serves to illustrate an important point: although the global annual mean radiative forcing is a widely used predictor of climate change, this metric may not be suitable in cases where the forcing agent is unevenly distributed in space and/or season. Stratospheric ozone depletion is thus a prime example of an external perturbation for which the global mean radiative forcing is a very poor indicator of the associated climate-system response.

It is well established that the absorption of incoming solar UV radiation by stratospheric ozone heats the stratosphere, and thus the observed ozone depletion (Figure 2) is expected to be accompanied by a decrease in stratospheric temperatures. This stratospheric cooling has indeed been observed over Antarctica, as shown in Figure 3. The cooling is largest (∼8 K between 1960 and 2000) during austral spring (September–October–November (SON)), coinciding with the season of maximum ozone depletion (Figure 2). A somewhat smaller cooling has been observed during summer (December–January–February (DJF)). In addition to stratospheric ozone depletion, increasing concentrations of well-mixed GHGs are also expected to lead to stratospheric cooling. Unlike the very seasonal nature of ozone forcing, however, the GHG increases occur throughout the year (Table 1). The lack of any significant temperature trends during austral autumn (March–April–May (MAM)) and winter (June–July–August (JJA)) in Figure 3 therefore suggests that increasing GHGs had a

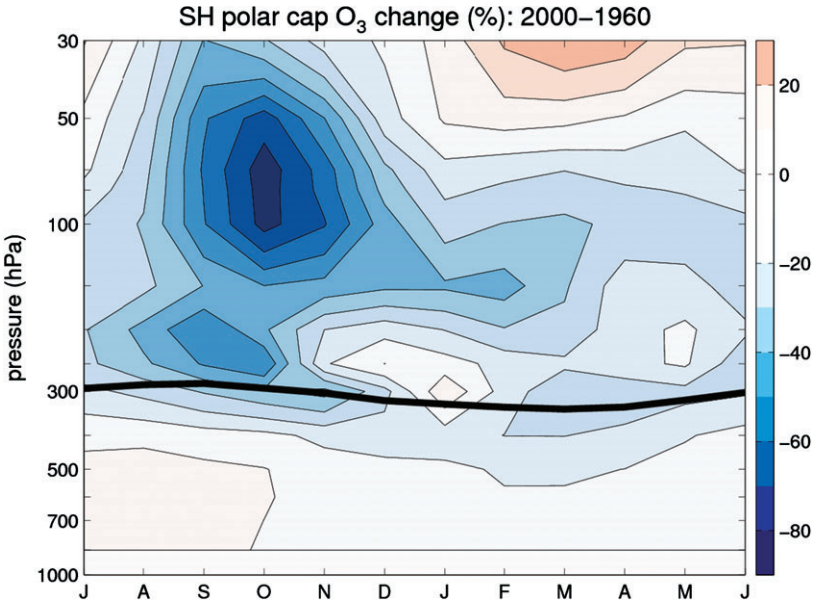

Figure 2. AC&C/SPARC (Cionni *et al.*, 2011) ozone changes (in %; 1996–2005 mean minus 1956–1965 mean) averaged over the SH polar cap (70–90°S). The thick black contour represents the 1981–2010 mean tropopause position (defined as the pressure on the 2-PVU surface) based on ERA-Interim reanalysis data (Dee *et al.*, 2011).

Table 1. Comparison of forcing characteristics.

	Stratospheric O_3	GHGs
Global annual mean RF[a]	-0.05 ± 0.10	$+2.6 \pm 0.3$
Geographic region	High latitude SH[b]	Global
Season	SH springtime	All seasons
Time history	Depletion from 1970s to 2000, with projected recovery by $\sim$ 2050[c]	Monotonic increase

[a]Stratospheric-adjusted radiative forcing (RF, in W m^{-2}, with 90% confidence range) in 2005 relative to pre-industrial (Forster *et al.*, 2007).
[b]Stratospheric ozone depletion has occurred globally, but severe depletion (i.e., the ozone 'hole') is restricted to the Southern Hemisphere (SH) polar region.
[c]Approximate date when Antarctic October mean total column ozone is projected to return to 1980 levels (Eyring *et al.*, 2010).

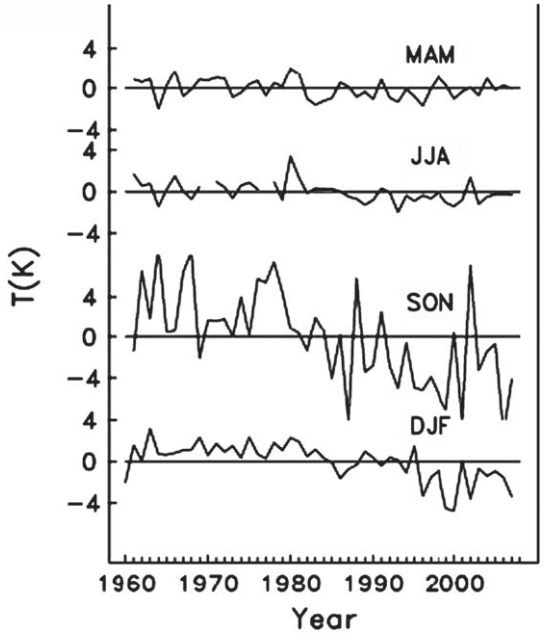

Figure 3. Observed seasonal mean 100 hPa temperature anomalies averaged over the Antarctic region (from Randel *et al.*, 2009).

relatively small impact on polar lower stratospheric temperatures in the late twentieth century*. The dramatic stratospheric cooling that was observed in SON and DJF is thus primarily a response to ozone depletion (Randel *et al.*, 2009). This ozone-induced cooling is reproduced in the current generation of coupled atmosphere–ocean general circulation models (GCMs) and coupled chemistry–climate models (CCMs; Young *et al.*, 2013). The cooling has important implications for the atmospheric circulation in the SH, as discussed in the next section.

2.2. *Atmospheric circulation changes*

The cooling of the Antarctic lower stratosphere during spring due to ozone depletion increases the meridional temperature gradient at tropopause levels between the polar region and SH midlatitudes. Thermal wind balance requires this increased temperature gradient to be accompanied by increased vertical shear of the geostrophic wind. This is manifest as a strengthening of the stratospheric 'polar vortex' (or polar-night jet), the band of westerly winds encircling the polar cap. Such a strengthening of the polar vortex has been observed in recent decades (e.g. Waugh *et al.*, 1999; Thompson and Solomon, 2002). The vortex has also become more persistent (Waugh *et al.*, 1999), meaning that its seasonal breakdown and the associated final warming of the polar lower stratosphere have occurred later in the austral spring (by about 2 weeks between the late 1970s and late 1990s). The delayed breakdown of the polar vortex acts to prolong and deepen the seasonal Antarctic ozone hole, by maintaining the cold temperatures in the polar lower stratosphere that are necessary for PSC formation and rapid ozone loss (Solomon, 1999).

These changes in the stratospheric circulation are dynamically coupled to tropospheric circulation changes, with the latter lagging the former by 1–2 months. The tropospheric circulation response to ozone depletion thus occurs primarily during austral summer (DJF). In simple terms: the band of strongest westerly winds associated with the tropospheric jet shifts poleward, with a related poleward shift in the storm track.

*It should also be noted that GHG-induced stratospheric cooling amplifies with height, but it is relatively small in the lower stratosphere (Manabe and Wetherald, 1967).

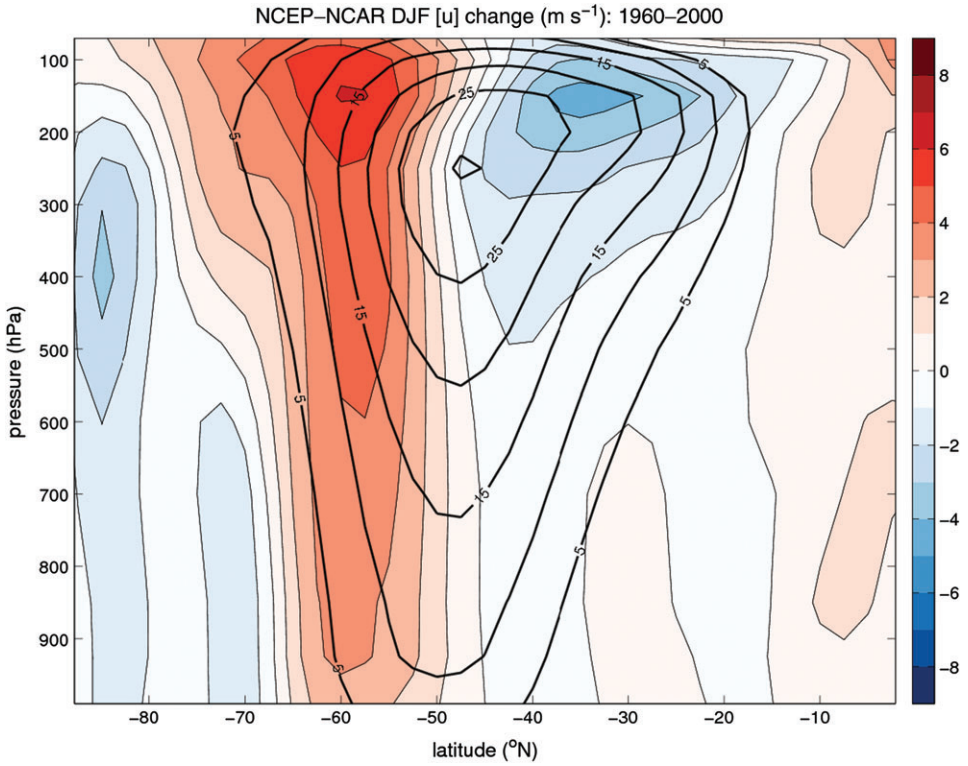

Figure 4. DJF zonal-mean zonal wind change (shading) during 1960–2000 based on NCEP/NCAR reanalysis data (Kalnay *et al.*, 1996). The contour interval is 1 m s^{-1}. Thick black contours depict the climatological zonal-mean zonal wind (in m s^{-1}) during this period.

This is illustrated in Figure 4, which shows the DJF zonal-mean zonal wind change between 1960 and 2000 based on data from the National Centers for Environmental Prediction/National Center for Atmospheric Research (NCEP/NCAR) reanalysis (Kalnay *et al.*, 1996). (Results are similar for other reanalyses.) A prominent acceleration of the westerly flow is seen on the poleward side of the climatological tropospheric jet, with a corresponding deceleration of the westerlies equatorward of the jet. This pattern of zonal wind change indicates a poleward shift in the jet position. We estimate the magnitude of this shift to be ∼2–3° of latitude between 1960 and 2000 based on the location of the 850 hPa zonal-mean zonal wind maximum (not shown). This is comparable to the SH jet-shift simulated by the latest generation of coupled atmosphere–ocean GCMs during the period of ozone depletion (Barnes *et al.*, 2014).

The poleward shift in the tropospheric jet was accompanied by a poleward shift in the extratropical storm tracks, as inferred from the observed decreases in cyclone activity at SH midlatitudes (Simmonds and Keay, 2000) and increases at high latitudes (Wang *et al.*, 2013). Changes in the mean meridional circulation have also been observed in recent decades. In particular, the subsiding branch of the zonal-mean Hadley circulation in the SH during DJF has shifted poleward by ∼1–3° of latitude (depending on the reanalysis dataset used) between 1979 and the first decade of the current century (Hu and Fu, 2007).

These atmospheric circulation changes are often described as a trend toward the positive phase of the Southern Annular Mode (SAM), which is the leading mode of variability of the SH extratropical circulation (Thompson and Wallace, 2000). The positive phase of the SAM is manifested in different ways in the stratosphere and troposphere (Gerber and Polvani, 2009). In the former, the SAM trend describes the observed strengthening of the lower stratospheric polar-night jet, and in the latter it reflects the observed poleward shift of the tropospheric jet. In other words, the SAM is nothing more than a proxy for variability in the jets.

Various methods for computing the SAM have been used in the literature. For example, it is common to define the SAM as the first empirical orthogonal function (EOF) of the SH extratropical geopotential height or zonal-mean zonal wind (at different levels in the troposphere and stratosphere; e.g. see Thompson and Wallace, 2000). In this case, the principal component time-series associated with the first EOF is taken to be the SAM index. A more straightforward, and physically meaningful, SAM index can be computed simply as the anomalous zonal-mean sea-level pressure (SLP) difference between SH high and middle latitudes (e.g. Marshall, 2003). During the positive phase of the SAM, this SLP difference is enhanced relative to the climatological mean, which corresponds to an intensification of the circumpolar westerly winds.

Whether phrased as a jet shift or as a positive SAM trend, multiple lines of evidence suggest that the observed tropospheric circulation changes in the SH in the late twentieth century are primarily a response to stratospheric ozone depletion. One indication of this comes from the seasonality of the observed changes. The recent positive trend in the SAM (i.e. poleward shift in the tropospheric jet and storm tracks) is statistically significant only during the austral summer and autumn seasons, with insignificant trends during winter and spring (Marshall, 2007). Similarly, the observed poleward expansion of the SH Hadley cell is significant only in DJF and MAM (Hu and Fu, 2007). The seasonality of these changes strongly points to stratospheric ozone depletion as a major driving factor, at least for the changes observed in DJF. The delay between the maximum ozone depletion in austral spring and the tropospheric circulation response in summer is consistent with the approximate time required for the downward propagation of stratospheric circulation anomalies (Baldwin and Dunkerton, 1999, 2001; Thompson *et al.*, 2005). In contrast, it is not obvious that the observed tropospheric circulation trends in MAM should be directly linked with stratospheric ozone depletion. Fogt *et al.* (2009) have suggested instead that these MAM trends are largely a manifestation of internal climate variability.

Additional strong evidence for the importance of stratospheric ozone depletion in driving recently observed SH circulation changes comes from model simulations. These model simulations can be grouped into three categories. The first consists of idealized atmospheric GCM simulations forced with an imposed cooling of the polar stratosphere (Polvani and Kushner, 2002; Kushner and Polvani, 2004; Gerber and Polvani, 2009; Butler *et al.*, 2010). This cooling effectively mimics the occurrence of ozone depletion, and the idealized context allows for robust and easily reproducible exploration of how stratospheric cooling affects the tropospheric circulation. The second and third categories consist of simulations with more realistic models, including stand-alone atmospheric GCMs, coupled atmosphere–ocean GCMs, and coupled CCMs. Here, stratospheric ozone depletion is imposed directly (i.e. rather than imposing the associated cooling), either by changing ozone concentrations (in GCMs), or by changing emissions of ODSs (in CCMs). In the second category, ozone (or ODS) forcing is specified in isolation, so no ambiguity exists as to the cause of the simulated climate change (Sexton, 2001; Gillett and Thompson, 2003; Shindell and Schmidt, 2004; Arblaster and Meehl, 2006; Sigmond *et al.*, 2010; McLandress *et al.*, 2011; Polvani *et al.*, 2011b). The third category includes so-called 'ensembles of opportunity' (e.g. simulations performed for the Coupled Model Intercomparison Project, phase 3 (CMIP3)), in which ozone (or ODS) forcing is specified in combination with other forcings, most notably well-mixed GHGs (Miller *et al.*, 2006; Cai and Cowan, 2007; Karpechko *et al.*, 2008; Fogt *et al.*, 2009; Son *et al.*, 2009, 2010). In this case, the relative importance of ozone depletion and GHG increases in driving the model-simulated circulation changes is inferred by examining the seasonality of these changes (as discussed above), and by comparing simulations with both ozone and GHG forcing to simulations with GHG forcing alone (i.e. in which ozone depletion does not occur).

Figure 5 shows an example of modelled DJF zonal-mean zonal wind change between 1960 and 2000 based on one particular modelling study (Polvani *et al.*, 2011b) that used an atmospheric GCM: the NCAR Community Atmosphere Model, version 3 (CAM3). Four 50-year time-slice integrations with CAM3 were performed: (i) a 1960 control integration (labelled REF1960 in Figure 5) with stratospheric ozone, well-mixed GHGs, sea-surface temperatures (SSTs) and sea-ice concentrations (SICs) specified based on observations; (ii) an 'ozone only' integration (OZONE2000) with stratospheric ozone set to its observed year 2000 levels, and GHGs, SSTs and SICs kept at 1960 levels; (iii) a 'GHG only' integration (GHG2000) with year 2000 GHGs, SSTs and SICs, and stratospheric ozone held fixed at 1960 levels; and (iv) an 'all forcings' integration (BOTH2000) with stratospheric ozone, well-mixed GHGs, SSTs and SICs all set to year 2000 levels.

When the full set of forcings is imposed in the CAM3 in the BOTH2000 experiment, the model simulates a pronounced acceleration (deceleration) of the westerly flow on the poleward (equatorward) side of the climatological tropospheric jet (Figure 5(c)). This is in good agreement with the observed zonal wind changes (Figure 4) and clearly shows a poleward shift of the jet during the 1960–2000 period. The model-simulated circulation changes that occur when all forcings are included (Figure 5(c)) are very similar to the changes in response to ozone depletion alone (Figure 5(a)). The GHG increases also contribute to the circulation changes (Figure 5(b)), but their contribution is small in comparison to that of ozone depletion[†]. The CAM3 also simulates a clear poleward expansion of the Hadley cell in the SH during DJF 1960–2000, similar to what was observed (not shown). This Hadley cell expansion is likewise predominantly a response to stratospheric ozone depletion (see also Min and Son, 2013). From such evidence, the only conclusion is that ozone depletion has been the dominant driver of recently observed atmospheric circulation changes in the SH during summer,

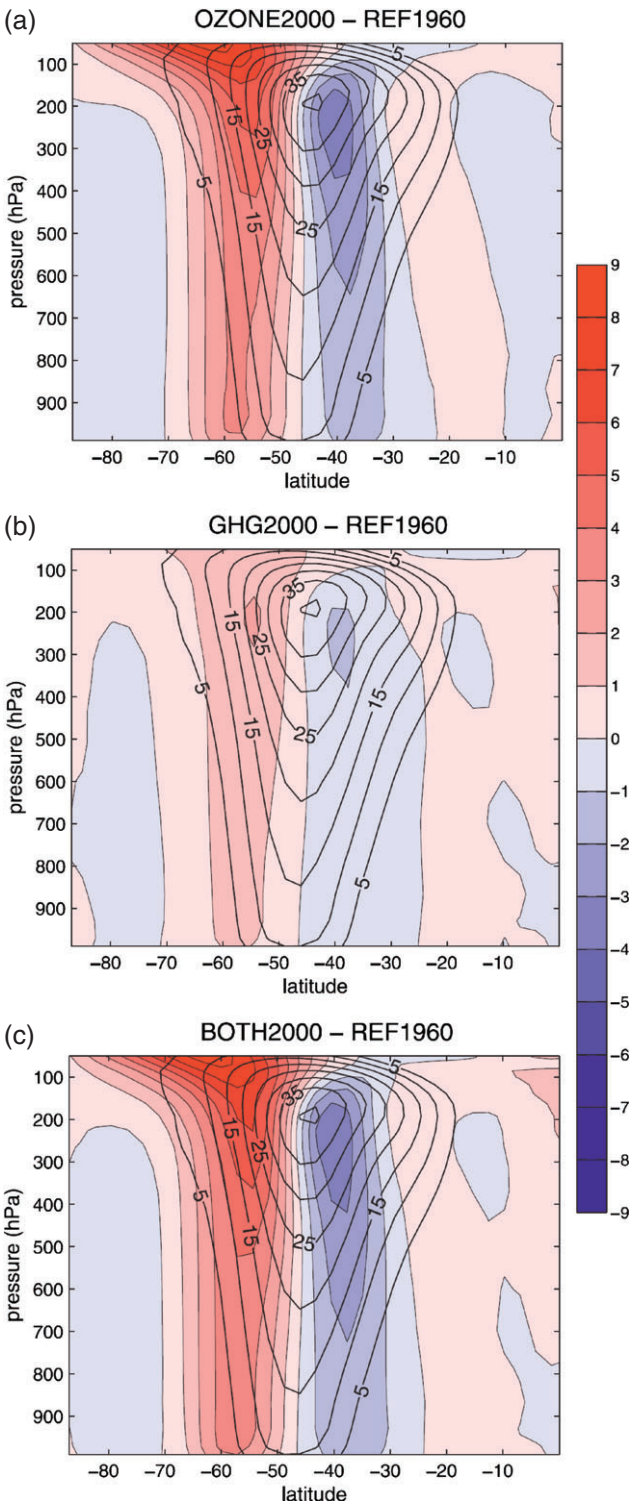

Figure 5. The CAM3 simulated DJF zonal-mean zonal wind response (shading, with a contour interval of 1 m s^{-1}) to (a) stratospheric ozone depletion, (b) GHG increases, and (c) both. Black contours depict the climatological zonal-mean zonal wind (in m s^{-1}) in the REF1960 integration (from Polvani *et al.*, 2011b).

[†]In CAM3, the poleward shift of the tropospheric jet induced by ozone depletion is roughly 2-3 times larger than that induced by increasing GHGs. This dominant role of ozone depletion in shifting the jet was confirmed in a recent observational study (Lee and Feldstein, 2013), although in this study the ozone contribution was estimated to be only 50% greater than the contribution from GHGs.

with the GHG increases only playing a secondary role. We emphasize that this conclusion is not based solely on CAM3 results, but is substantiated by the large number of observational and modelling studies cited above.

The poleward shift of the tropospheric jet, and the associated atmospheric circulation changes that were observed in the late twentieth century, have contributed significantly to many other climate changes, as will be discussed in subsequent sections. Here, we briefly describe how these ozone-induced climate changes can be quantified using the SAM as a simple metric to represent the jet shift (see also Thompson *et al.*, 2011).

Consider the change in some climate variable x (e.g. surface temperature, precipitation) over some specified period of time. The component of this change that is congruent with the SAM trend can be expressed as: $dx = r_{x:\mathrm{SAM}} \times d\mathrm{SAM}$, where $r_{x:\mathrm{SAM}}$ is the regression of x on to the SAM index (typically estimated using detrended monthly or seasonal mean data)[‡], and dSAM is the linear trend in the SAM index over the specified time period. As the observed late twentieth century SAM trend (in summer) was primarily due to stratospheric ozone depletion (see above), the climate response of the variable x to ozone depletion is well approximated using dx. Thus, in the discussion that follows, we will document how various aspects of SH climate probably responded to the recent trend in the SAM, with the understanding that this describes to a very large degree the response to ozone depletion itself.

There are a few caveats with this approach that are worth noting. First, it is assumed that the relationship between the SAM and x on month-to-month and year-to-year time-scales (i.e. as given by $r_{x:\mathrm{SAM}}$) will hold on multidecadal time-scales as well. Second, as noted earlier, the observed SAM trend in the late twentieth century is not a response to stratospheric ozone depletion alone; increasing GHGs (and possibly other factors) also make a small contribution to this trend. Finally, although many of the stratospheric ozone effects on climate are mediated through the SAM, this is not true in all cases. We will provide examples below of where changes in the SAM are, in fact, a poor predictor of the climate response to ozone forcing.

2.3. *Tropospheric and surface temperature changes*

The observed poleward intensification of the tropospheric jet discussed in the previous section is expected, based on thermal wind balance, to be accompanied by an enhanced tropospheric temperature gradient between the Antarctic region and SH midlatitudes. In accordance with this, both radiosonde (Thompson and Solomon, 2002) and satellite (Johanson and Fu, 2007) measurements have documented Antarctic tropospheric cooling during summer and autumn in the late twentieth century. The region of cooling is surrounded by a band of tropospheric warming at midlatitudes (Johanson and Fu, 2007). A qualitatively different pattern of tropospheric temperature trends emerges during austral winter and spring. In these seasons, cooling is replaced by warming over most of Antarctica. This warming tends to exceed the warming occurring in the midlatitude troposphere (Fu *et al.*, 2006; Johanson and Fu, 2007), indicating a reduction in the meridional temperature gradient.

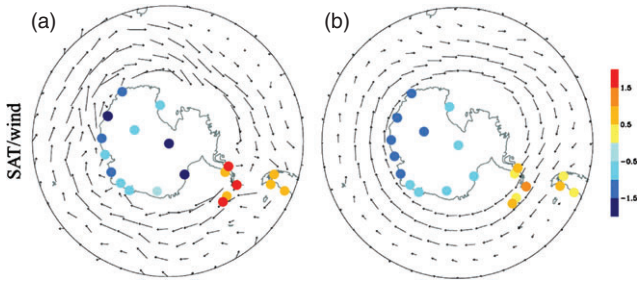

Figure 6. December–May trends (a) and the contribution of the SAM to the trends (b). Surface air temperature (SAT) trends (1969–2000) are plotted as coloured circles, with a contour interval of 0.5 K per 30 years. The 925 hPa wind trends (1979–2000) are plotted as vectors, with the longest vector corresponding to ~4 m s^{-1} (from Thompson and Solomon, 2002).

Therefore, as for the tropospheric circulation changes discussed above, the observed tropospheric temperature changes bear a distinct seasonality that reflects the seasonally varying stratospheric ozone forcing. Ozone depletion may contribute to the observed tropospheric temperature trends during summer in at least two ways. First, the forced positive trend in the SAM and related poleward shift of the tropospheric circulation sets up a pattern of anomalous ascent at high latitudes and anomalous descent at midlatitudes, which adiabatically cools the polar troposphere and warms the midlatitude troposphere[§] (Thompson *et al.*, 2003). Second, the observed summertime cooling of the polar troposphere may be driven in part by a decrease in downwelling long-wave (LW) radiation resulting from ozone-induced cooling of the overlying stratosphere (Grise *et al.*, 2009).

The impact of stratospheric ozone depletion is also seen in surface-temperature trends in recent decades. Perhaps the most dramatic and widely studied of these surface temperature trends are those that occurred over Antarctica, illustrated in Figure 6(a)[¶]. Surface warming of more than 1.5 K is seen over the Antarctic Peninsula during the 1969–2000 period, with cooling of a similar magnitude occurring over parts of East Antarctica. Somewhat less warming is evident over Patagonia. Additionally, although not apparent from Figure 6(a) due to the lack of stations in the region, West Antarctica experienced surface warming during the second half of the twentieth century (Steig *et al.*, 2009). The magnitude of this warming, however, has been debated (O'Donnell *et al.*, 2011). Figure 6(b) shows the surface temperature change during 1969–2000 that is congruent with the positive trend in the SAM. The SAM trend accounts for roughly half of the observed surface warming over the Antarctic Peninsula, and nearly all of the observed cooling over East Antarctica (Thompson and Solomon, 2002). Much of the warming over Patagonia is also explained by the SAM.

The observed warming over the Antarctic Peninsula and Patagonia in recent decades is the result of increased warm temperature advection from the Southern Ocean due to intensified near-surface westerly winds (Thompson and Wallace, 2000; Thompson and Solomon, 2002; van den Broeke and van Lipzig, 2004; Marshall *et al.*, 2006), as indicated by the vectors in Figure 6. Warming over West Antarctica has been linked with a deepening of the Amundsen Sea Low (Steig *et al.*, 2009), which might be related to ozone depletion (Turner *et al.*, 2009).

[‡]The regression coefficient, $r_{x:\mathrm{SAM}}$, measures the strength of the relationship between the climate variable x and the SAM on month-to-month and year-to-year timescales. It is typically estimated using an ordinary least-squares approach, in which a regression line is fit through the (detrended) time-series scatter plot of x versus the SAM index. The slope of this regression line then defines $r_{x:\mathrm{SAM}}$.

[§]This mechanism would also be expected to contribute to the observed tropospheric temperature trends during autumn, given the positive SAM trend in this season; however, the autumn SAM trend does not appear to be forced by ozone depletion.

[¶]Shown in the figure are surface temperature trends during the months of December through to May; however, the observed trends are very similar if DJF is considered alone (not shown).

Finally, east Antarctic cooling has been attributed to a suppression of the katabatic flow over the ice sheet due to anomalous rising motion during the positive phase of the SAM (Thompson and Wallace, 2000; van den Broeke and van Lipzig, 2004).

The observed pattern of surface warming over the Antarctic Peninsula, West Antarctica and Patagonia, and cooling over East Antarctica, is well reproduced in model simulations forced solely by stratospheric ozone depletion (McLandress *et al.*, 2011), indicating that ozone depletion has played a central role in producing these temperature trends. Ozone depletion is also expected to have contributed to late twentieth century summertime warming in the south of New Zealand, and cooling over central and eastern subtropical Australia, based on the observed interannual relationship between the SAM and surface temperature in these regions (Gillett *et al.*, 2006; Hendon *et al.*, 2007). These ozone-induced temperature anomalies may have been driven in part by changes in clouds and cloud radiative effects associated with the poleward shift of the tropospheric jet (Grise *et al.*, 2013; see section 2.4). However, Gillett *et al.* (2006) note that outside of the Antarctic, the actual observed surface-temperature changes in recent decades do not strongly resemble the changes that would be predicted based on the SAM trend. This suggests either that the SAM–surface-temperature relationship is different on interannual and multidecadal time-scales, or (more likely) that the SAM (i.e. ozone) impact on temperatures has been overwhelmed by other factors (e.g. increasing GHGs).

2.4. *Cloud and precipitation changes*

In this final section on the atmospheric response to stratospheric ozone depletion, we discuss the implications of the observed poleward shift of the tropospheric circulation for cloud cover and precipitation in the SH during summer. The cloud response to ozone depletion was recently examined by Grise *et al.* (2013) using the CAM3 GCM. They carried out four 100 year time-slice integrations of the model. These included 1960 control, 'ozone only', 'GHG only' and 'all forcings' (i.e. both ozone and GHGs) integrations. The integrations are nearly identical to those performed by Polvani *et al.* (2011b) using CAM3 (see section 2.2), with the exception of the simulation length (100 years versus 50 years), and the fact that Grise *et al.* (2013) employed a version of CAM3 that was coupled to a slab ocean and thermodynamic sea ice model (i.e. rather than prescribing SSTs and SICs).

Similar to the Polvani *et al.* (2011b) result for the tropospheric circulation (e.g. see Figure 5), Grise *et al.* (2013) found that the CAM3 simulated cloud changes in DJF in the 'all forcings' integration closely resembled the cloud changes in response to ozone depletion alone. In the 'ozone only' integration, high- and mid-level clouds increase at high southern latitudes and decrease at midlatitudes as a result of the poleward shift of the tropospheric jet and storm tracks. Low-level cloud changes are of opposite sign, with decreases simulated at high latitudes and modest increases simulated at midlatitudes. In the SH Subtropics, there is an increase in high and mid-level cloud fraction as a consequence of the poleward shift of the Hadley circulation. The Hadley cell shift creates a region of anomalous divergence in the subtropical upper troposphere, which leads to anomalous rising motion and enhanced cloud formation (Kang *et al.*, 2011). The CAM3 simulated cloud changes in response to ozone depletion are similar to those seen in satellite observations during periods when the tropospheric jet is anomalously poleward (Grise *et al.*, 2013).

Figure 7 shows the DJF top-of-atmosphere (TOA) radiation anomalies due to cloud changes in the CAM3 'ozone only' integration. The anomalies were computed using the cloud radiative kernels of Zelinka *et al.* (2012). The LW cloud-induced radiation anomalies (Figure 7(a)) are due to changes in high- and mid-level clouds. The temperature of these clouds is much lower than the surface temperature, and thus changes in their distribution significantly affect the outgoing long-wave radiation (OLR) at the TOA. Increases in high- and mid-level clouds at polar latitudes and in the Subtropics lead to reduced OLR (i.e. positive LW radiation anomalies), whereas decreases in these clouds at midlatitudes produce opposite-signed LW anomalies.

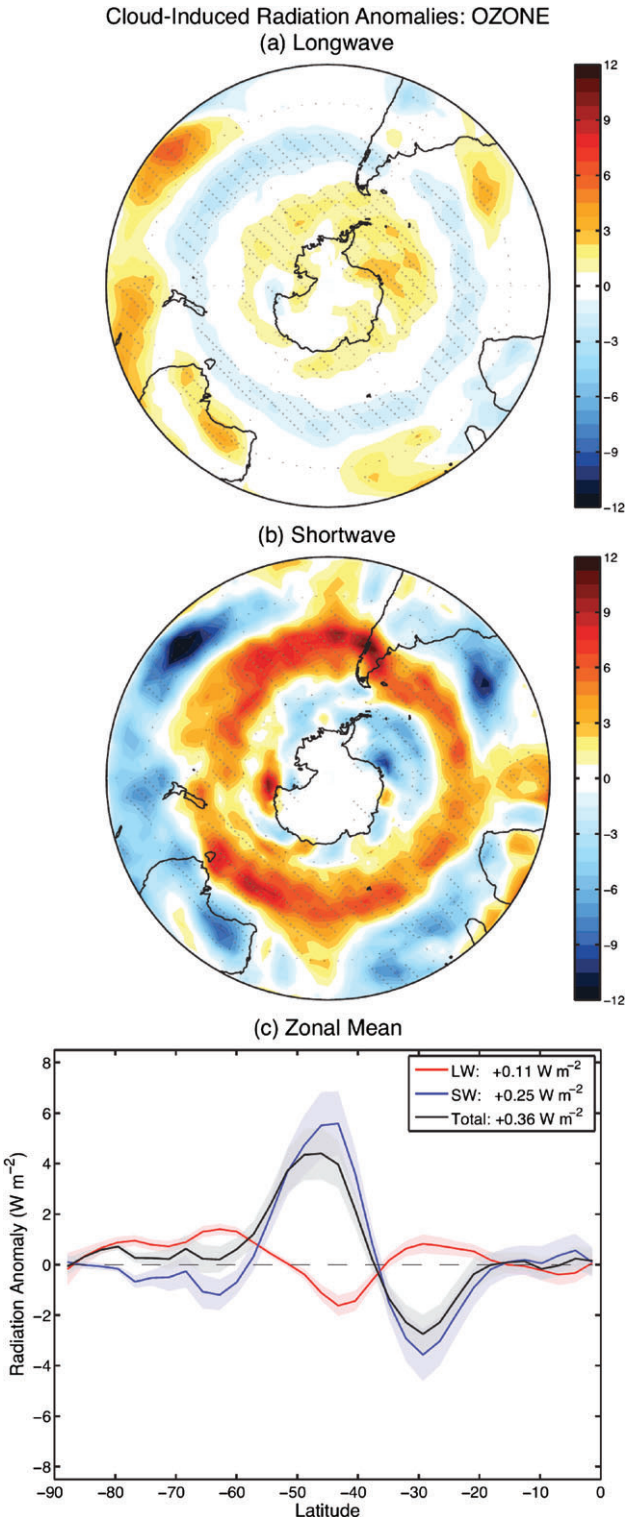

Figure 7. DJF cloud-induced TOA radiation anomalies (in W m^{-2}) simulated by CAM3 in response to prescribed stratospheric ozone depletion. TOA longwave (LW) and shortwave (SW) anomalies are plotted in (a) and (b), respectively. Panel (c) shows the zonal-mean LW, SW and total (LW + SW) responses, with the legend in the upper right indicating the hemispherically averaged values (from Grise *et al.*, 2013).

The shortwave (SW) cloud-induced radiation anomalies (Figure 7(b)) are a reflection of changes in the total cloud fraction, which are dominated by high- and mid-level cloud changes in the CAM3. Accordingly, subtropical and polar regions with increased high- and mid-level cloudiness are characterized by a reduction in the absorbed solar radiation (ASR) within the atmosphere–surface column (i.e. negative TOA SW anomalies). In contrast, ASR increases substantially at midlatitudes in association with reduced high- and mid-level cloud amounts. These midlatitude SW anomalies could contribute to the poleward shift of the maximum meridional surface temperature gradient and eddy-driven jet over the Southern Ocean (Grise *et al.*, 2013; see also Ceppi *et al.*, 2012).

The zonal-mean cloud-induced radiation anomalies are shown in Figure 7(c). At high latitudes, anomalies in the LW and SW largely cancel one another, resulting in a small positive total (LW + SW) radiation anomaly at the TOA. This is not the case at midlatitudes and in the Subtropics, however, where total radiation anomalies are dominated by large increases and decreases in ASR, respectively. Averaged over the entire SH, the total cloud-induced radiation anomaly at the TOA in DJF is +0.36 W m^{-2}, with positive contributions from both the LW (+0.11 W m^{-2}) and SW (+0.25 W m^{-2}). This illustrates an important point: the total radiative impact of stratospheric ozone depletion depends significantly on the dynamic feedbacks that are induced, and not just on the direct radiative forcing. Although the latter is largely confined to the region of the Antarctic ozone hole, the former can be significant throughout much of the SH.

The cloud responses simulated by the CAM3 are physically consistent with expectations based on our understanding of how the tropospheric circulation responds to stratospheric ozone depletion. However, another indication that the simulated cloud changes are realistic, at least in a qualitative sense, comes from the fact that they are similar to observed precipitation changes in the late twentieth century. Figure 8 shows the observed zonal-mean precipitation change during DJF 1979–2000 (red curve), along with the component of this precipitation change that is congruent with the positive trend in the SAM (blue curve). In accordance with the changes in high- and mid-level clouds discussed above, total precipitation increases at high latitudes and in the Subtropics (with local maxima near 60°S and 30°S), and decreases at midlatitudes (with a local minimum near 40°S). The basic latitudinal structure of these precipitation changes, and a significant part of their amplitude, can be explained by the positive trend in the SAM, as indicated by the overall close correspondence between the red and blue curves in Figure 8. The observed precipitation changes in Figure 8 are also very similar to the changes simulated by models that were forced solely by stratospheric ozone depletion (Kang *et al.*, 2011). It should be noted, however, that model simulations do not reproduce the strong decrease in precipitation that is seen in the observations near 10°S, suggesting that this feature is probably not a response to stratospheric ozone forcing.

Finally, it is important to point out that the zonal-mean precipitation changes in Figure 8, which are dominated by changes occurring over the ocean, are representative of many of the observed land precipitation changes in recent decades. For example, observed summertime decreases in precipitation over most of New Zealand (Figure 9(a)) typify the overall drying at midlatitudes caused by the positive trend in the SAM (Figure 8). The SAM trend also accounts for a significant portion of the trend in New Zealand precipitation (Figure 9(b)). In the mountainous western regions of the South Island, 30–60% of the observed drying is congruent with the SAM, with more than 80% of the precipitation trend explained by the SAM in some regions of the North Island (Ummenhofer *et al.*, 2009). In contrast to the drying over New Zealand, summertime increases in precipitation were observed in the late twentieth century over southeastern Australia and southeastern South America. These precipitation increases similarly have been linked to the positive trend in the SAM, and therefore, ultimately, to stratospheric ozone depletion (Hendon *et al.*, 2007; Gonzalez *et al.*, 2013).

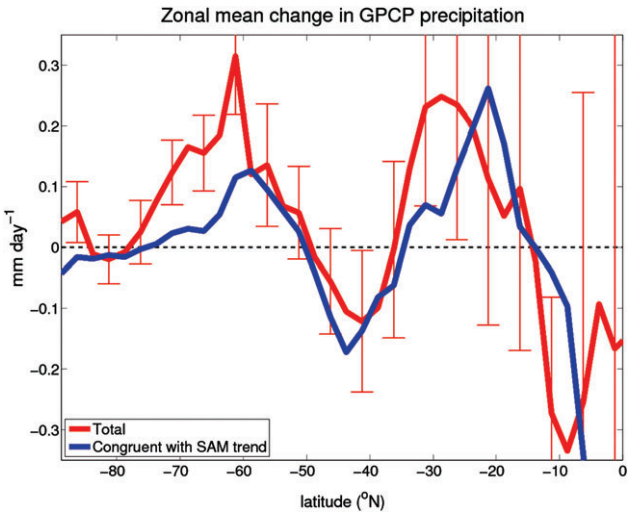

Figure 8. Zonal-mean change in GPCP (Global Precipitation Climatology Project) DJF precipitation during 1979–2000. The total precipitation change is plotted in red, and is based on the linear trend in the seasonal-mean precipitation at each latitude. The component of the precipitation change that is congruent with the SAM trend is plotted in blue. Error bars bracket the plus and minus one standard deviation range of the detrended seasonal-mean data, providing an indication of the year-to-year precipitation variability.

3. Oceanic response to stratospheric ozone depletion

3.1. *Ocean circulation changes*

The westerly winds that blow over the Southern Ocean play a fundamental role in driving the oceanic circulation. Thus, ocean circulation changes might be expected to occur in response to the poleward intensification of the westerlies brought about by stratospheric ozone depletion. In this section, we discuss whether these changes in ocean circulation have in fact been observed.

In a climatological sense, the westerly wind stress acting on the surface of the Southern Ocean creates a region of Ekman divergence and upwelling on the poleward side of the surface wind maximum, and convergence and downwelling equatorward of the maximum. This wind-driven overturning has the effect of steepening the isopycnals (surfaces of constant density) in the meridional direction, thus implying a build up of potential energy in the ocean due to the winds. The resulting north–south density gradient is associated with the eastward-flowing, surface-intensified Antarctic Circumpolar Current (ACC), which is the largest ocean current on the planet. The ACC and the meridional overturning circulation (MOC) in the Southern Ocean thus represent a tightly coupled system that is driven largely by the SH westerly winds. Southern Ocean upwelling on the poleward flank of the ACC plays a critical role in the global MOC by being the primary route through which deep waters that are formed at high latitudes (e.g. in the North Atlantic) return to the surface (Marshall and Speer, 2012). This implies a close connection between the upwelling and climate, because the former will determine the rate at which deep-ocean reservoirs of heat and carbon communicate with the surface.

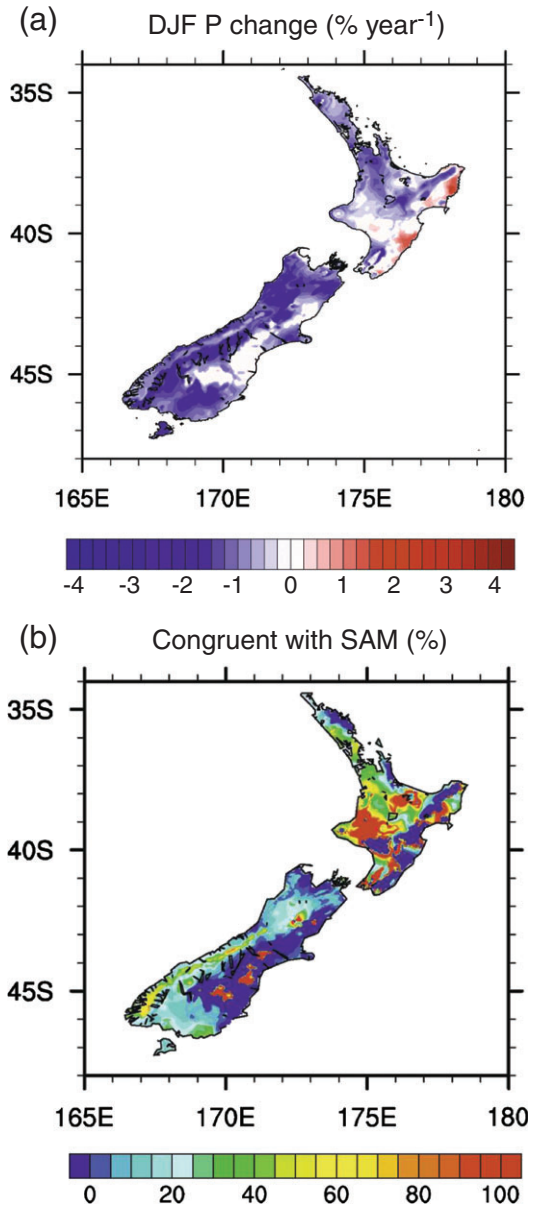

Figure 9. (a) Observed New Zealand precipitation change during DJF 1979–2000. (b) Percentage of the precipitation change that is congruent with the trend in the SAM (from Ummenhofer *et al.*, 2009).

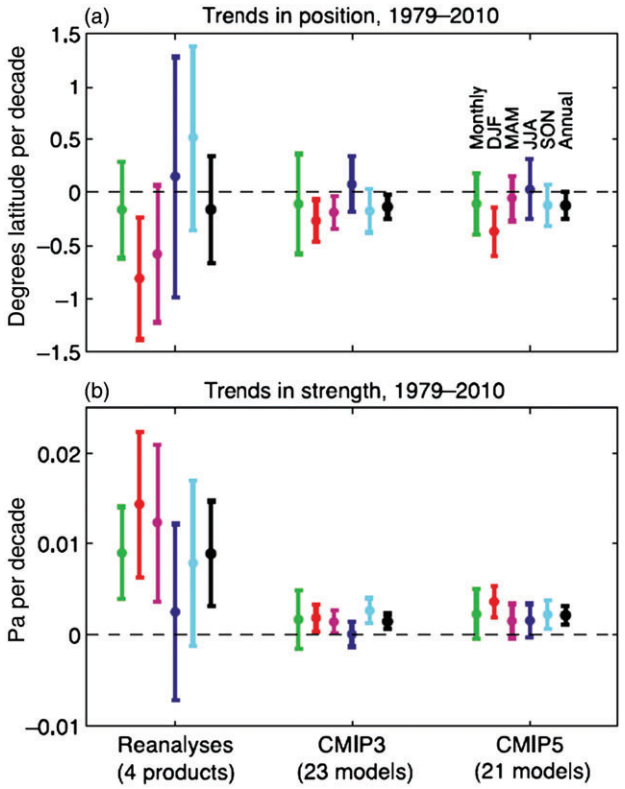

Figure 10. Observed (average of four reanalysis products) and model-simulated trends in (a) position and (b) strength of the SH surface westerly wind-stress maximum during 1979–2010. The error bars show the 95% confidence interval of the trends, where auto-correlation has been accounted for (from Swart and Fyfe, 2012).

How have the ACC and Southern Ocean MOC been affected by the recent poleward intensification of the westerlies brought about by ozone depletion? The westerly wind changes are expected to be accompanied by changes in the position and strength of the maximum zonal wind stress over the Southern Ocean. Figure 10 indicates that this is indeed the case. In both atmospheric reanalyses and climate models, a statistically significant poleward shift and strengthening of the surface westerly wind stress is evident during DJF 1979–2010. The wind-stress changes in DJF are in almost all cases larger in magnitude than the changes in other seasons. (The latter changes are typically not even statistically significant.)

The only exception to this occurs for the trend in wind-stress strength as simulated by the coupled atmosphere–ocean GCMs that participated in the CMIP3. In the CMIP3 models, the greatest strengthening of the surface westerly wind stress during the 1979–2010 period occurs in the SON season. We note, though, that only about half of the CMIP3 models included stratospheric ozone depletion in their simulations. In the newer generation CMIP5 models, which all included ozone depletion, the greatest strengthening trend in the wind stress is simulated in DJF, in agreement with reanalyses. However, despite this improvement in the CMIP5, Figure 10 indicates that there remains a systematic tendency for the models to underestimate the observed trends in wind-stress position and strength. This alone would tend to produce an unrealistically small change in ocean circulation in the models. (As will be discussed below, however, ocean circulation changes depend on other factors besides the change in surface wind stress.) Nevertheless, models and reanalyses agree at least qualitatively that there has been a poleward shift and intensification of the surface westerly wind stress over the Southern Ocean in recent decades. The seasonality of these changes clearly suggests that they were largely driven by stratospheric ozone depletion.

In response to the ozone-induced changes in the surface wind stress, an enhancement of the northward Ekman transport across much of the Southern Ocean can be expected. The stronger Ekman flow contributes to increased upwelling of upper Circumpolar Deep Water (CDW) south of the ACC, and to increased downwelling of Subantarctic Mode Water (SAMW) and Antarctic Intermediate Water (AAIW) north of the ACC. This strengthening of the MOC implies an increase in the tilt of isopycnals across the ACC, and thus an intensified ACC transport. The mean position of the ACC is also expected to shift poleward along with the maximum in the surface westerly wind stress.

Such behaviour of the Southern Ocean circulation has been simulated in models in response to poleward intensified westerly winds (Bi *et al.*, 2002; Hall and Visbeck, 2002; Saenko *et al.*, 2005; Fyfe and Saenko, 2006; Sen Gupta and England, 2006; Sigmond *et al.*, 2011). The crucial caveat, however, is that the models used do not resolve oceanic mesoscale eddies. (We note, though, that eddy effects are parametrized in the models.) These eddies, with a characteristic spatial scale of ∼100 km, are known to play a critical role in the ocean circulation. Eddy fluxes largely counteract the

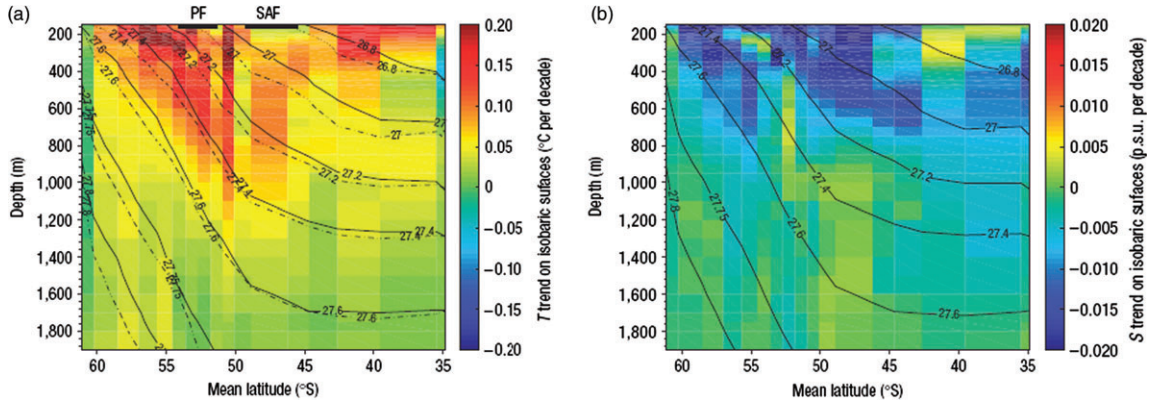

Figure 11. Observed trends in (a) potential temperature and (b) salinity between the 1960s and 2000s. Black contours in (a) represent the mean position of the isopycnals at the beginning (solid contours) and end (dashed contours) of this period. Black bars in (a) indicate the average latitudes of the polar front (PF) and subantarctic front (SAF). In (b), the mean climatological isopycnal surfaces are denoted by black contours (from Böning *et al.*, 2008).

effects of Ekman pumping, and the balance between these two processes (or residual circulation) defines the upper cell of the Southern Ocean MOC (Marshall and Speer, 2012). Thus, the MOC and ACC transport may have been rather insensitive to the recent multidecadal changes in the winds caused by ozone depletion, due to compensation between changes in Ekman transport and eddy fluxes. Satellite observations indicate that poleward intensified westerly winds do induce, with a lag of 2–3 years, an increase in eddy activity in the ACC (Meredith and Hogg, 2006). This effect has also been simulated in high-resolution models that are able to adequately capture the eddy field (Henning and Vallis, 2005; Hallberg and Gnanadesikan, 2006; Hogg *et al.*, 2008; Screen *et al.*, 2009; Treguier *et al.*, 2010; Abernathey *et al.*, 2011). The resulting increase in southward eddy transport in these models was found to largely offset the increase in northward Ekman transport, producing little change in the strength of the MOC.

We now assess whether oceanographic observations provide any evidence for an ozone-induced strengthening of the Southern Ocean MOC and ACC transport in recent decades. Figure 11 shows the observed zonal-mean temperature and salinity changes across the ACC between the 1960s and 2000s. Multidecadal warming and freshening trends extending to depths of more than 1000 m are evident over the entire latitudinal extent of the ACC. The upper-ocean warming is greatest in the southern portion of the ACC in the area near and south of the polar front (PF). This feature has also been noted in model simulations (Fyfe *et al.*, 2007; Hogg *et al.*, 2008; Screen *et al.*, 2009), and has been attributed to an increase in poleward eddy heat flux. The overall structure of the temperature and salinity changes in Figure 11 is consistent with a warming and freshening of surface waters due to altered surface buoyancy fluxes, and the subsequent subduction of these warm and fresh anomalies along isopycnals[‖] (Böning *et al.*, 2008).

Changes in temperature and salinity together determine how the density field in the ocean changes, with important implications for the ocean circulation. The evolution of the density field between the 1960s and 2000s can be inferred from Figure 11(a), which shows the mean position of the isopycnals at the beginning (solid lines) and end (dashed lines) of this period. The most prominent feature is a broad-scale subsidence of the isopycnal surfaces across the ACC. At depths of 800–1000 m in the vicinity of the PF and subantarctic front (SAF), this subsidence exceeded 50 m during the past 40 years, which is equivalent to a southward shift of about 50–80 km (Böning *et al.*, 2008). This southward shift implies a similar shift in the mean position of the ACC, which is expected based on the changes in surface wind stress (Figure 10(a)). However, although the isopycnal surfaces have moved downward and poleward, there is no indication from Figure 11(a) of a systematic increase in their tilt across the ACC. As discussed above, the isopycnal tilt, and associated north–south density gradient, are closely related to the strength of the MOC and ACC transport. Based on these results then, it might be tempting to conclude that these aspects of the Southern Ocean circulation have changed relatively little in recent decades in response to stratospheric ozone depletion.

Analyses of additional observational data prevent such a definitive conclusion, however. In a recent study, Waugh *et al.* (2013) used oceanic measurements of CFC-12, which acts as a passive tracer in the ocean, to infer decadal-scale changes in the Southern Ocean MOC. Their results are shown in Figure 12. Observed *p*CFC-12 (CFC-12 partial pressure) values in 1991 are greatest in surface waters due to the anthropogenic origin of this compound (Figure 12(a)). The locations of two of the primary water masses of the ACC are noted: upper CDW that upwells south of the PF, and SAMW that ventilates the thermocline north of the SAF. Figure 12(b) shows the observed change in *p*CFC-12 between 1991 and 2005. Increases in *p*CFC-12 occur everywhere in accordance with the increase in atmospheric concentrations during this period. The largest increase is seen in the subtropical thermocline near the core of the SAMW.

The crucial question is whether or not it is necessary to invoke changes in ocean circulation in order to explain the observed *p*CFC-12 changes. To this end, Waugh *et al.* (2013) adopted a modelling approach in which the circulation was constrained to remain fixed between 1991 and 2005. Under this assumption of steady transport, two very different transport models were used to simulate the spatiotemporal evolution of CFC-12 in the ocean, given its observed atmospheric time history. Differences between modelled and observed *p*CFC-12 changes would then be indicative of a change in transport during the 1991–2005 period.

The simulated *p*CFC-12 changes are shown in Figure 12(c) and (d). Increases in *p*CFC-12 that are smaller than observed are evident in the subtropical thermocline, while larger-than-observed *p*CFC-12 increases occur in the models in the CDW upwelling regime. It thus appears that the observed *p*CFC-12 changes (Figure 12(b)) are not consistent with steady transport. Instead, the observed *p*CFC-12 increases in the subtropical thermocline (which are larger than predicted by

[‖]The observed warming and freshening at the ocean surface is also reflected in changes in the properties of the water masses that comprise the ACC (i.e. upper CDW, SAMW and AAIW; see Böning *et al.*, 2008).

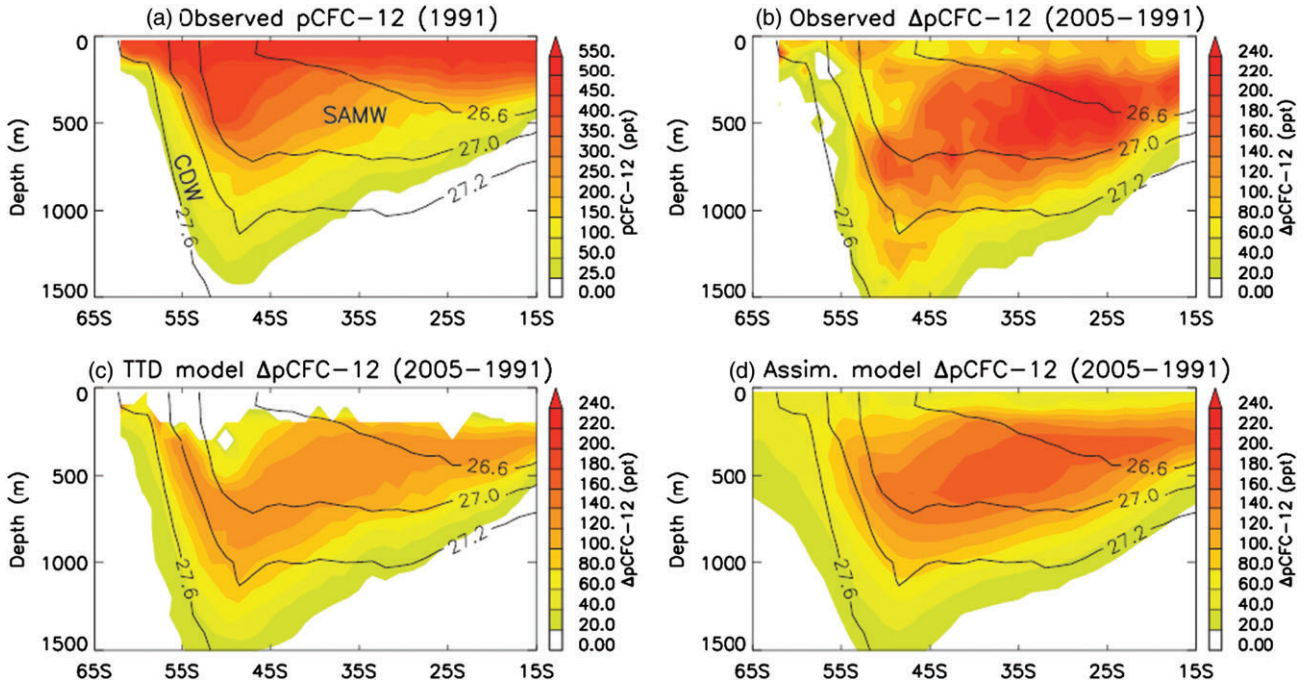

Figure 12. (a) Observed depth-latitude distribution of *p*CFC-12 (CFC-12 partial pressure) in 1991. The locations of Circumpolar Deep Water (CDW) and Subantarctic Mode Water (SAMW) are indicated. (b) Observed change in *p*CFC-12 between 1991 and 2005. (c,d) Simulated *p*CFC-12 change between 1991 and 2005 based on two transport models assuming steady transport. In all panels, black contours denote the mean position of the isopycnal surfaces (from Waugh *et al.*, 2013).

the models) suggest an enhancement of thermocline ventilation rates, implying transport of younger (i.e. more recently ventilated) waters with higher amounts of CFC-12 into the ocean interior. Similarly, the smaller-than-predicted *p*CFC-12 increases in polar waters suggest an enhancement of CDW upwelling rates, implying increased transport of older waters that are depleted in CFC-12 to the ocean surface. In other words, the differences between modelled and observed changes in *p*CFC-12 support the idea that stratospheric ozone depletion has caused some strengthening of the Southern Ocean MOC in recent decades. As discussed in the next section, this idea is further supported by recent changes in the Southern Ocean uptake of atmospheric CO_2.

3.2. *Changes in Southern Ocean CO_2 uptake*

Among other reasons, it is important to know whether or not the Southern Ocean circulation has changed during the past few decades because of the key role it plays in the cycling of carbon between ocean and atmosphere. Southern Ocean upwelling south of the PF brings water that is rich in dissolved inorganic carbon to the surface, thereby promoting outgassing of natural CO_2 to the atmosphere. This is countered by the uptake of anthropogenic CO_2 by SAMW and AAIW, and the subsequent subduction of these water masses into the thermocline north of the SAF. The latter process is significant: over the past two centuries, ∼40% of the global oceanic uptake of anthropogenic CO_2 has occurred in the Southern Ocean (Sabine *et al.*, 2004; Mikaloff Fletcher *et al.*, 2006). The net Southern Ocean CO_2 air–sea flux therefore reflects the balance between outgassing of natural CO_2 and uptake of anthropogenic CO_2. A perturbation to either of these components (e.g. due to a change in ocean circulation) could have implications for atmospheric CO_2 concentrations, and thus global climate.

Le Quéré *et al.* (2007) used an inverse method to estimate the spatiotemporal evolution of the net (natural + anthropogenic) CO_2 air–sea flux over the global ocean during 1981–2004. The trend in the CO_2 flux over the Southern Ocean (i.e. poleward of 45°S) is shown in Figure 13. Case I represents the standard inversion, with the other black and grey coloured bars denoting a number of sensitivity tests that were performed. (See Le Quéré *et al.* (2007) for details; the sensitivity tests Is1, Is3 and Is5 produced the best match to station measurements of atmospheric CO_2 concentration.) With one exception, all inversions indicate that there has been a positive trend in the Southern Ocean CO_2 air–sea flux during the 1981–2004 period, signifying a reduction in the net oceanic uptake of atmospheric CO_2. This positive trend was reproduced in an ocean general circulation model (OGCM) that was forced with observed changes in surface winds and heat and freshwater fluxes (blue bar in Figure 13). The observed weakening of the Southern Ocean CO_2 sink stands in stark contrast to what would be expected from the increase in atmospheric CO_2 concentration alone. As indicated by the red bars in Figure 13, the atmospheric CO_2 increase would be expected to enhance oceanic CO_2 uptake (resulting in a negative trend in the CO_2 air–sea flux), contrary to what was observed. Differences between the observed CO_2 flux trend (i.e. the inversions) and the trend predicted based on the increase in atmospheric CO_2 alone are statistically significant at the 92.5% level or higher in all cases (and at greater than the 99% level in most cases).

The observed weakening of the Southern Ocean CO_2 sink has been attributed to the recent poleward intensification of the westerlies, and a consequent strengthening of the Southern Ocean MOC (Le Quéré *et al.*, 2007; Lovenduski *et al.*, 2008). The stronger MOC is purported to have led to an increase in the outgassing of natural CO_2 as a result of more vigorous upwelling of carbon-rich CDW. Although this effect probably has been offset by an increase in the Southern Ocean uptake of anthropogenic CO_2 (due mainly to the increase in atmospheric CO_2 concentration), the changes in the natural CO_2 flux have been dominant, and thus the net oceanic CO_2 uptake has declined. The link between the observed changes in the CO_2 air–sea flux and the poleward intensification of the westerly winds points directly to stratospheric ozone depletion as a prime driver of the CO_2 flux changes.

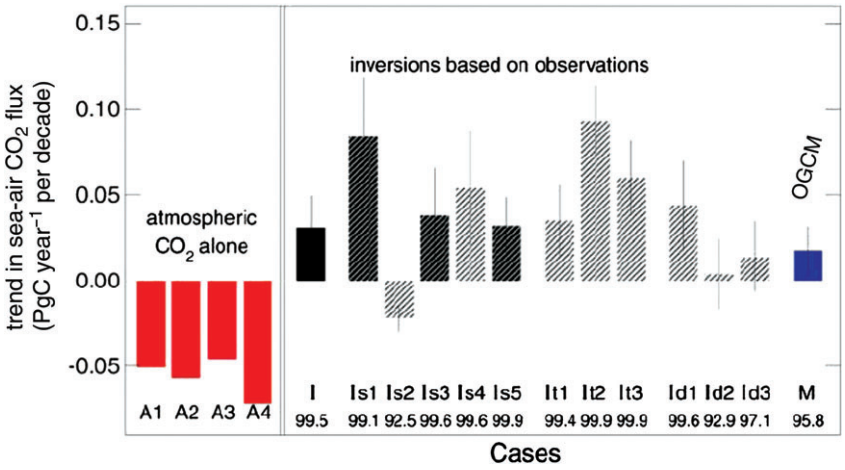

Figure 13. Trends in the annually integrated Southern Ocean CO_2 air-sea flux between 1981 and 2004 from inversions based on observations (black and gray bars) and an ocean general circulation model (OGCM) forced with observed changes in surface winds and heat and freshwater fluxes (blue bar). See text for additional details. Red bars denote the CO_2 flux trend that would be expected based on the increase in atmospheric CO_2 alone. The statistical significance of the CO_2 flux trend for the different cases (relative to the trend expected from the atmospheric CO_2 increase alone) is indicated by the numbers on the bottom right (from Le Quéré *et al.*, 2007).

In order to investigate this further, Lenton *et al.* (2009) carried out two ensembles of simulations with a coupled climate–carbon cycle model, one ensemble that included prescribed stratospheric ozone depletion, and a second ensemble that did not. The two ensembles were identical in all other respects, thus allowing for clear identification of the effect of ozone depletion on the CO_2 air–sea flux. When ozone depletion was included in their model, Lenton *et al.* (2009) found that the Southern Ocean uptake of atmospheric CO_2 was reduced relative to the case without ozone depletion. Furthermore, this reduced CO_2 uptake was shown to be a response to enhanced ventilation of carbon-rich deep water (and associated increased outgassing of natural CO_2) due to poleward intensified westerly winds. As noted above, this same mechanism has been invoked to explain the observed changes in the CO_2 air–sea flux over the Southern Ocean in recent decades (Le Quéré *et al.*, 2007). These modelling results therefore lend support to the notion that stratospheric ozone depletion has weakened the Southern Ocean sink for atmospheric CO_2.

4. Cryospheric response to stratospheric ozone depletion

4.1. *Antarctic sea-ice changes*

The discussion in the previous section on recent changes in the Southern Ocean naturally leads one to question how these changes may have affected Antarctic sea ice. In the satellite era, total Antarctic sea-ice extent (SIE) has exhibited a small but statistically significant positive trend, with an estimated magnitude of 0.127×10^6 km^2 per decade during 1979–2005 (Parkinson and Cavalieri, 2012; Turner *et al.*, 2013). Given that stratospheric ozone depletion has had a marked impact on many aspects of SH climate over this period, it is logical to suspect that ozone depletion may have played a role in the observed sea-ice expansion.

However, despite these expectations, it has been argued that the observed Antarctic sea-ice changes cannot be explained by the positive trend in the SAM (Lefebvre *et al.*, 2004; Liu *et al.*, 2004; Simpkins *et al.*, 2012). This suggests either that the sea-ice response to ozone depletion is not mediated through the SAM, or that the observed sea-ice expansion is due to mechanisms other than stratospheric ozone depletion. Regarding the former possibility, Turner *et al.* (2009) have suggested that ozone depletion induces a non-annular (i.e. zonally asymmetric) atmospheric circulation response (a deepening of the Amundsen Sea Low), which may help to explain the observed autumn increases in sea ice in the Ross Sea in recent decades.

A more direct way to assess the impact of stratospheric ozone depletion on Antarctic sea ice is to use coupled atmosphere–ocean GCM experiments in which ozone depletion is the only prescribed external forcing. Such experiments were carried out by Sigmond and Fyfe (2010) and by Bitz and Polvani (2012), with results from the latter study shown in Figure 14. Bitz and Polvani (2012) examined the Antarctic climate response to ozone depletion using two different versions of a coupled model: one version that was run at 0.1° horizontal resolution for the ocean and sea-ice components, and a second version that used a much coarser 1° resolution for the ocean and sea ice. (The atmospheric and land-surface components of the model were identical in both cases.) Thus, in the 0.1° case, oceanic mesoscale eddies are explicitly permitted by the model, whereas these eddies are parametrized in the 1° case.

In response to ozone depletion, the annual-mean sea-ice concentration (SIC) is simulated to decrease over most of the Southern Ocean at both model resolutions (Figure 14(a) and (b)). (Note, however, that localized areas of SIC increase are not statistically significant.) The ice loss tends to occur mainly near the edge of the ice pack (thick black contour in the figures) in the 1° case, and is more broadly distributed in the 0.1° case. Figure 14(c) and (d) shows the response of the total Antarctic SIE as a function of month. Also plotted are the simulated (green lines) and observed (red lines) SIE climatologies, indicating that the model generally does a good job in reproducing the seasonal cycle of Antarctic sea ice (particularly at 0.1° resolution). The total Antarctic SIE decreases during every month of the year at both model resolutions, with greater month-to-month variability in the response in the 0.1° model version. In the annual mean, the magnitude of the simulated ice loss has little dependence on resolution, being 0.77 and 0.85×10^6 km^2 in the 0.1° and 1° cases, respectively (corresponding to ∼6% of the total ice area). These results from Bitz and Polvani (2012) largely agree with the results of Sigmond and Fyfe (2010), although some differences between the two studies do exist in terms of the magnitude of the modelled sea-ice loss.

The decrease in Antarctic sea ice due to stratospheric ozone depletion, in these model simulations, is partly driven by dynamics. Poleward intensified westerly winds induce an

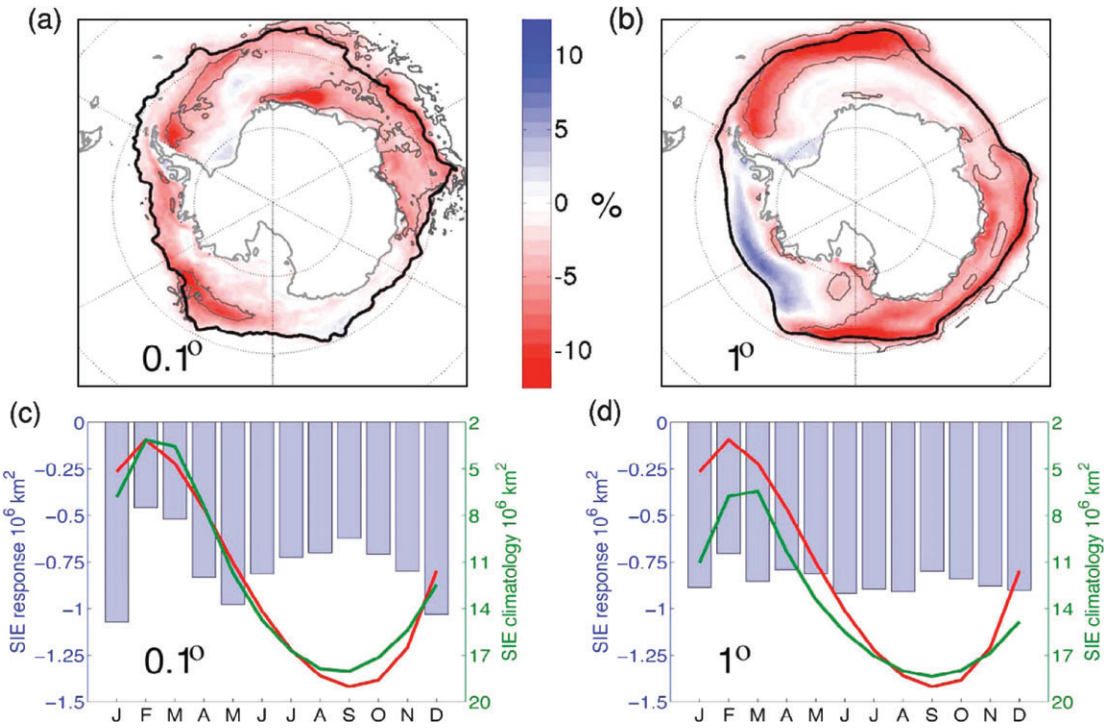

Figure 14. (a) Change in annual-mean sea-ice concentration (SIC) in response to stratospheric ozone depletion, as simulated by the NCAR Community Climate System Model, version 3.5 (CCSM3.5). The CCSM3.5 was run using a horizontal resolution of 0.1° for the ocean and sea-ice components. The thick black contour marks the winter (JJA) sea-ice 15% concentration, and the thin black contours indicate regions where the SIC response is significant at the 95% confidence level. (b) As in (a), but using a 1° horizontal resolution for the ocean and sea-ice. (c) Change in total Antarctic sea-ice extent (SIE) in response to stratospheric ozone depletion, using the 0.1° model version. The curves denote the SIE climatology in the model (green line) and observations (red line). (d) As in (c), but for the 1° model version (from Bitz and Polvani, 2012).

anomalous northward Ekman drift in the ocean surface layer, which acts to advect ice away from the Antarctic continent. This contributes to decreases in SIC in the near-coastal waters during DJF. However, the bulk of the simulated ice loss in the Southern Ocean is the result of thermodynamic processes, specifically a warming of the upper ocean that leads to increased basal melting of the sea ice. The ocean warming and thus the ice loss occur throughout the year (e.g. see Figure 14(c,d)), indicating that the ocean–ice system is an effective integrator of the highly seasonal stratospheric ozone forcing. Upper-ocean warming in the model is primarily a response to two mechanisms, originally identified in Sigmond and Fyfe (2010). First, stronger westerly winds in summer enhance upper-ocean mixing, which entrains warmer water from depth into the surface layer. The surface warming and sea-ice loss are amplified by a positive ice-albedo feedback. Second, the model shows a strengthening of the Southern Ocean MOC in response to poleward intensified westerlies, implying enhanced upwelling of warm water south of the PF. Differences in the simulated ocean warming between the 0.1° and 1° model versions occur as a result of differences in the eddy heat flux response. However, these differences tend to be greatest equatorward of the sea-ice edge, and thus they have little impact on the simulated ice loss. This makes the sea-ice response to ozone depletion less dependent on model resolution than might have been expected (Bitz and Polvani, 2012).

The results of coupled GCM experiments therefore suggest that the observed expansion of Antarctic sea ice during the satellite era cannot be explained by stratospheric ozone depletion. This expansion is also at odds with the expectation of diminishing ice cover in response to GHG-induced warming. Climate model simulations driven by all known natural and anthropogenic forcings indicate that the total Antarctic SIE should have declined in recent decades, in contrast to what has been observed (Arzel *et al.*, 2006; Maksym *et al.*, 2012; Turner *et al.*, 2013). An alternative explanation, suggested recently by Polvani and Smith (2013), is that the recent sea-ice expansion is not a forced response, but instead is a reflection of internal variability within the climate system (see also Mahlstein *et al.*, 2013; Zunz *et al.*, 2013).

4.2. *Changes in the mass balance of the Antarctic ice sheet*

The Antarctic ice sheet is presently losing mass at a rate of about 250 ± 31 Gt year^{-1}, which is equivalent to 0.7 mm year^{-1} of global sea-level rise (Rignot, 2011). This mass loss has been increasing during the past couple of decades at a rate of 14 ± 2 Gt year^{-2}. The recent acceleration of ice sheet mass loss is not thought to be due to changes in snowfall and/or ice melt, but rather to the acceleration of outlet glaciers in several key sectors of the ice sheet. Glaciers on the Antarctic Peninsula accelerated by as much as 300–800% following the collapse of the Larsen A and B ice shelves (Rignot *et al.*, 2004; Domack *et al.*, 2005), and have maintained high velocities since. In the Amundsen Sea sector of West Antarctica, outlet glaciers have also sped up in recent decades. For example, Pine Island Glacier accelerated by 80% in 35 years (Rignot, 2011). Glacier acceleration in this sector of the ice sheet has been attributed to the presence of warm CDW that drives large rates of bottom melt near the grounding lines (Rignot, 1998; Shepherd *et al.*, 2004; Thomas *et al.*, 2004).

It is not inconceivable that stratospheric ozone depletion may have contributed to the recent changes in the mass balance of Antarctica. For instance, the warming over the Antarctic Peninsula during the past few decades (which was at least partly driven by ozone depletion; see section 2.3) probably contributed to the 2002 collapse of the Larsen B ice shelf (Marshall *et al.*, 2006). Ozone depletion has also been linked to enhanced upwelling of warm CDW (Waugh *et al.*, 2013), which (as noted above) has played a role in the recent acceleration of outlet glaciers in

the Amundsen Sea region. Apart from these dynamic changes, there is reason to expect that ozone depletion might have had an impact on the surface mass balance (SMB) of the ice sheet, given observed relationships between the SAM and Antarctic snow accumulation and summertime melt (Thomas *et al.*, 2008; Tedesco and Monaghan, 2009). Although the SMB has not exhibited any long-term trend in recent decades (Monaghan *et al.*, 2006; van den Broeke *et al.*, 2006), this does not necessarily imply a negligible ozone impact. We discussed in section 4.1 how the tendency of ozone depletion to melt Antarctic sea ice has apparently been overwhelmed by some other factor (possibly internal variability), resulting in an overall positive trend in the observed SIE in the late twentieth century. Similarly, ozone depletion could indeed have had an effect on ice sheet SMB that was masked by other competing effects. Future work is needed to determine this.

5. Climate-system response to stratospheric ozone recovery

Up to this point, we have focused exclusively on the climate system response to stratospheric ozone depletion in the late twentieth century. However, the recovery of stratospheric ozone is anticipated during the next several decades as atmospheric concentrations of ODSs continue to decline in response to the implementation of the Montreal Protocol. We discuss in this section the expected impacts of ozone recovery on SH climate. Recall that the change in sign of the radiative forcing as ozone depletion transitions to ozone recovery is one of several ways in which stratospheric ozone forcing fundamentally differs from GHG forcing (see Table 1).

The time evolution of Antarctic October mean total-column ozone is shown in Figure 15 in observations (dotted black curve with error bars) and CCM simulations (coloured curves for individual models, and a thick black curve for the multimodel mean). When forced with the time history of ODS emissions, the CCMs reproduce the precipitous drop in total column ozone that is seen in the observations between 1960 and the turn of the century. These same models, when driven by projected future changes in ODS emissions, simulate a gradual recovery of ozone levels in the coming decades. In the multimodel mean, total-column ozone amounts over Antarctica are projected to return to 1980 levels by around 2050 (red vertical dashed line), with some uncertainty in this return date (blue vertical dashed lines).

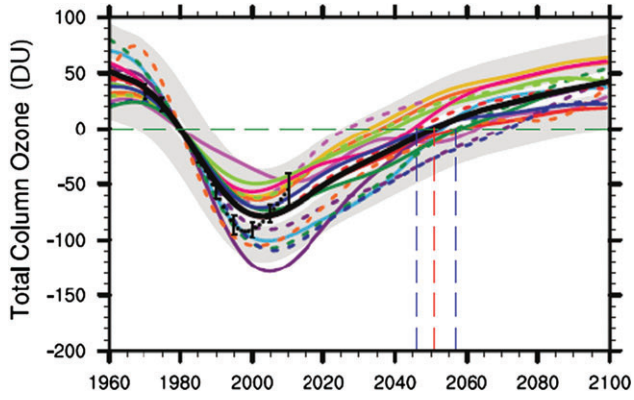

Figure 15. Antarctic October total column ozone (relative to 1980 levels) in observations (dotted black curve with error bars) and CCMVal-2 chemistry-climate model simulations (colored curves for individual models, and a thick black curve for the multi-model mean). The uncertainty in the multi-model mean time series is represented by gray shading. The red vertical dashed line indicates when the multi-model mean total column ozone returns to 1980 levels, with the blue vertical dashed lines denoting the uncertainty in this return date (from WMO, 2011).

Barring any substantial nonlinearities, the climate effects of stratospheric ozone recovery should be exactly opposite to the effects of ozone depletion. Thus, ozone recovery will favour an equatorward shift of the tropospheric circulation (the midlatitude jet and Hadley cell), and a negative trend in the SAM. This change in the sign of the climate response is important because it means that in the future, the effects of ozone recovery will oppose the effects of increasing GHGs. This is in contrast to the late twentieth century, when ozone depletion and GHG increases worked in the same direction to produce the observed positive trend in the SAM (and attendant changes). In the next several decades, the competing impacts of ozone recovery and increasing GHGs are expected to result in minimal forced changes in the atmospheric circulation during SH summer (Shindell and Schmidt, 2004; Son *et al.*, 2009, 2010; McLandress *et al.*, 2011; Polvani *et al.*, 2011a; Barnes *et al.*, 2014).

Figure 16 compares the simulated multimodel mean trends (based on several CCMs) in the DJF zonal-mean zonal wind during the periods 1979–1999 and 2000–2079. The CCMs were forced with observed (during 1979–1999) and projected (during 2000–2079) changes in GHGs, ODSs, SSTs and SICs. The projected GHG (ODS) changes were based on the A1B (A1) scenario, while the projected SSTs/SICs were taken from the A1B simulations of the CMIP3 coupled atmosphere–ocean GCMs. During the 1979–1999 period (Figure 16(a)), stratospheric ozone depletion, and to a much smaller extent GHG increases, have produced a strong acceleration of the westerly flow in the SH on the poleward side of the climatological tropospheric jet, implying a poleward shift in jet position (see section 2.2). This is very different than the projected future changes in the SH zonal wind (Figure 16(b)), which are much smaller due to large cancellation between the effects of ozone recovery and increasing GHGs.

This cancellation can also be visualized in terms of future changes in the SAM index. Figure 17 shows the SAM index during DJF 2001–2060 as simulated by the CAM3 (Polvani *et al.*, 2011a). In the ALL integrations (red lines), the CAM3 was forced with stratospheric ozone recovery, A1B GHG increases, and SST/SIC changes taken from a coupled atmosphere–ocean version of the same model under the A1B scenario. In contrast, only stratospheric ozone recovery was prescribed in the OZONE integrations (black lines), with all other forcings kept at year 2000 levels. Both the ALL and OZONE ensembles included 10 members each, differing only in their initial conditions. The difference between the multimember ensemble means (i.e. ALL minus OZONE) was used to estimate the effect of increasing GHGs, and the associated SST increase (thick blue line).

As discussed previously, stratospheric ozone recovery will favour a negative trend in the SAM in the coming decades (thick black line in Figure 17). Higher atmospheric GHG levels, on the other hand, will favour a continuation of the positive SAM trend (thick blue line) that was observed in the late twentieth century. The net effect of these two competing processes is expected to be a negligible trend in the austral summer SAM index during the next 50 years (thick red line). An important point here, however, is that this refers specifically to the forced response of the SAM. The spread of the individual model ensemble members (thin lines) in Figure 17 indicates that the internal variability of the extratropical circulation is very large (see also Deser *et al.*, 2012). Thus, unforced future changes in the SAM may occur that overwhelm any changes induced by external forcing. Indeed, this

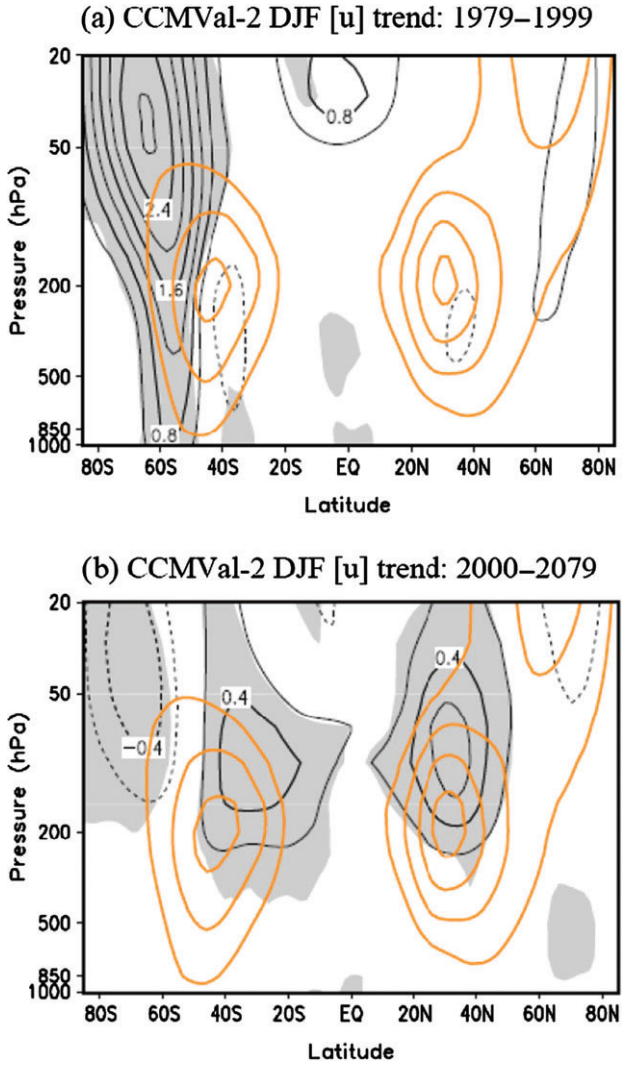

Figure 16. (a) The CCMVal-2 multimodel and zonal-mean zonal wind trend during DJF 1979–1999 in the REF-B1 scenario (black contours, with the contour interval of 0.4 m s^{-1} per decade). Trends exceeding one standard deviation are shaded. Orange contours represent the climatological zonal-mean zonal wind, with a contour interval of 10 m s^{-1} starting from 10 m s^{-1}. (b) As in (a), but for the zonal wind trend during DJF 2000–2079 in the REF-B2 scenario (from Son *et al.*, 2010).

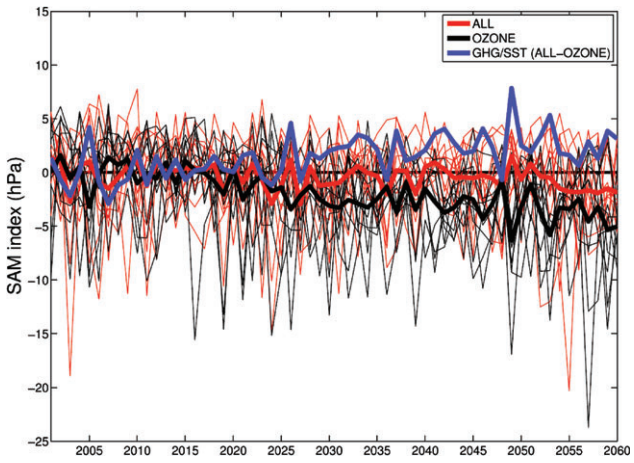

Figure 17. CAM3 simulated DJF SAM index during 2001–2060. The ALL integrations include both stratospheric ozone recovery and increases in GHGs (and associated sea surface temperature (SST) changes). Thin lines for the ALL and OZONE integrations represent individual ensemble members, while thick lines denote the multi-member ensemble means. The GHG/SST time series is calculated as the difference between the ALL and OZONE ensemble means (from Polvani *et al.*, 2011a).

may have taken place recently with regard to the observed changes in Antarctic sea ice (see section 4.1).

Two additional important points are worth noting. First, the tropospheric circulation effects of ozone recovery are expected to cancel the effects of increasing GHGs primarily in DJF, due to the strong seasonality of stratospheric ozone forcing** (see section 2). During the other seasons of the year, GHG forcing will act unopposed to shift the circulation poleward.

Second, even in DJF, the relative importance of ozone and GHG forcing for the tropospheric circulation depends significantly on the time period being considered. This is illustrated by Figure 18, which shows the CMIP5 simulated time series of midlatitude jet position and subtropical dry-zone edge in the SH during 1900–2099. (The dry zone edge is defined as the isopleth of precipitation (P) minus evaporation (E) equal to zero.) During the historical period of 1900–1970 (labelled HIST in the figure), the multimodel mean jet position and dry zone edge (thick black lines) are fairly constant. This is not terribly surprising, given that this period precedes the formation of the Antarctic ozone hole, and is also characterized by relatively weak GHG forcing. The situation changes dramatically during the subsequent 1970–2005 (O3DEPL) period, however. Here, ozone depletion and GHG increases (although mainly the former) produce a clear poleward shift (negative trend) in both the jet position and dry zone edge. Following this, during the 2005–2045 (O3RCVR) period, the circulation trends are again small, reflecting the cancellation between ozone recovery and increasing GHGs that is discussed above. This cancellation persists until mid-century, at which point the poleward shift of the circulation resumes during the FUTR period of 2045–2099, in response to the continued rise in atmospheric GHG amounts. Thus, although stratospheric ozone recovery will be a major future player in the climate system, its impacts will be felt primarily during the first half of the current century. In the second half of the century, when ozone recovery is mostly complete (see Figure 15), increasing GHGs are expected to be the dominant forcing driving SH climate change.

Finally, we have focused in this section on the tropospheric circulation effects of ozone recovery, because these are key to understanding many of the other climate impacts. However, not all aspects of the climate response to ozone forcing are mediated through tropospheric circulation changes (i.e. changes in the SAM). Figure 19 provides an example of this. Plotted are the 2001–2065 linear trends in the polar-cap (70–90°S) averaged TOA net (SW + LW) incoming radiation ((a) and (b)), and the horizontal convergence of the atmospheric energy transport ((c) and (d)), as simulated by the NCAR Community Earth System Model, version 1 (CESM1). The CESM1 was run using the high-top Whole Atmosphere Community Climate Model (WACCM) with interactive stratospheric chemistry as its atmospheric component. It also included a full dynamic ocean and a dynamic–thermodynamic sea-ice model (see Smith *et al.*, 2013, for details).

In response to twenty-first century stratospheric ozone recovery, the CESM1 projects an increase in the net incoming radiation at the TOA during most months of the year, with the largest increases occurring during austral spring (Figure 19(a)). In order to maintain atmospheric energy balance, changes in the TOA radiation over the Antarctic tend to be compensated, on annual and longer time-scales, by changes in the atmospheric

**It should be pointed out, however, that significant cancellation between ozone and GHG impacts on the ocean and sea ice is expected throughout the year (e.g. Smith *et al.*, 2012), because the ocean–ice system effectively integrates the highly seasonal ozone forcing.

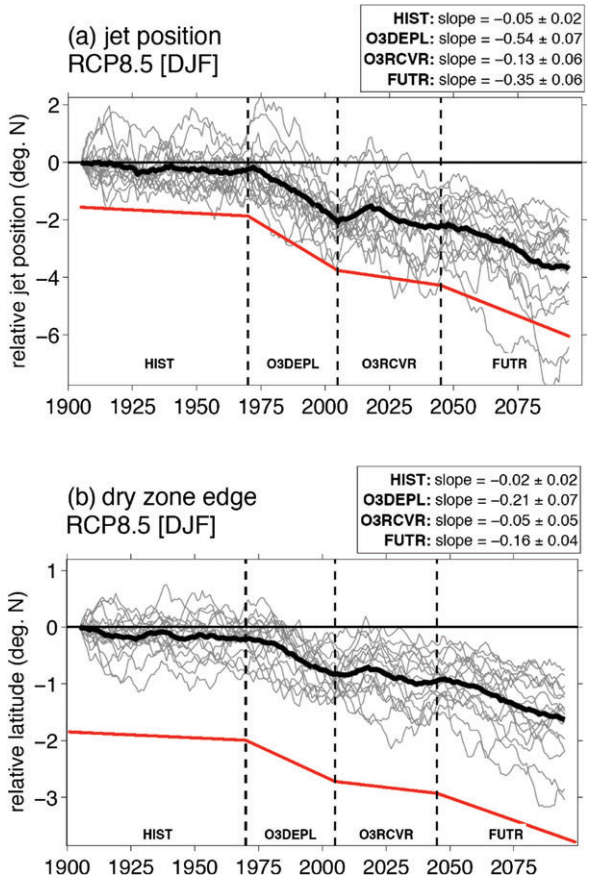

Figure 18. (a) Time series of the CMIP5 SH DJF jet position relative to the 1900–1910 value over the Historical and RCP8.5 scenarios. Gray curves denote the individual models and the multi-model mean is plotted in black. Red lines denote the piece-wise linear least-squares slopes, which are also given in the panel above in units of degrees per decade. Time series have been smoothed using a 10-year moving average filter. (b) As in (a), but for the latitude of the subtropical dry zone edge, defined as the isopleth of $P - E = 0$ (from Barnes *et al.*, 2014).

energy-flux convergence (Previdi *et al.*, 2013; Smith *et al.*, 2013). In accordance with this, decreases in the energy flux convergence over the polar cap are simulated throughout most of the year (Figure 19(c)), with the largest decreases lagging the largest increases in the TOA radiation by 2–3 months.

Figure 19(b) and (d) shows the TOA radiation and energy flux convergence changes that would be expected based on the model-simulated trend in the SAM. Despite the fact that the SAM is significantly correlated with these variables in the model on interannual time-scales (Smith *et al.*, 2013), it turns out to be a very poor predictor of the multidecadal changes considered here. In many cases, the TOA radiation and energy flux convergence changes that are predicted based on the SAM trend are of opposite sign to the changes actually simulated by the model (i.e. Figure 19(a) and (c)). The latter changes, therefore, cannot be explained by the SAM, and are a response to the direct radiative impacts of ozone recovery. Higher ozone amounts in the stratosphere lead to greater stratospheric absorption of SW radiation, primarily during austral spring. This increases the net incoming SW flux at the TOA, because the additional solar radiation absorbed within the stratosphere is no longer available to be reflected back to space by clouds and the surface. Although this effect is partly countered by enhanced OLR due to higher stratospheric temperatures, the changes in the SW are dominant, and thus the net TOA radiation increases during most months (Figure 19(a)). As noted above, these radiation increases are compensated for by decreases in the horizontal energy-flux convergence (Figure 19(c)), thereby maintaining the annual-mean energy balance of the polar atmosphere.

6. Summary and outlook

Anthropogenic climate change has become synonymous in many circles with the secular rise in atmospheric greenhouse gas concentrations resulting from human activity. For the SH, however, GHG-induced climate change is only one part of the story. In this review, we have documented the significant and widespread climate changes that have occurred in response to a very different anthropogenic forcing: stratospheric ozone depletion.

The climate impacts of ozone depletion are pervasive, extending from the stratosphere down to the surface (and possibly into the Southern Ocean), and from the Antarctic continent to the SH Subtropics. This fact is only beginning to be truly appreciated. Although significant and widespread climate changes have been observed in recent decades in the SH, and many of these changes have been linked to changes in the winds (notably, to the SAM), what has been missing is the following critical connection: because ozone depletion was the primary driver of the observed changes in the winds, it too, therefore, was the primary driver of the other observed climate changes that were a response to changes in the winds. In this review, we have sought to better emphasize this connection, which is particularly relevant for linking ozone depletion with changes in the Southern Ocean and possibly sea ice, and with changes at the surface in general.

The impact of ozone depletion on the SH climate system begins in the Antarctic lower stratosphere, where a substantial springtime cooling of ∼8 K has been observed over the last few decades of the twentieth century in response to the formation of the ozone hole (Figure 3). This cooling was the trigger for a series of atmospheric circulation changes, including a strengthening of the stratospheric polar vortex and tropospheric midlatitude jet, and a poleward shift of the tropospheric jet and Hadley cell. The changes in the tropospheric circulation, which are commonly described as a positive trend in the SAM, have been linked to changes in tropospheric and surface temperatures, clouds and cloud radiative effects, and precipitation. The seasonality of these climate changes in observations (with significant changes largely confined to austral summer) clearly suggests that they are primarily a response to stratospheric ozone depletion, rather than increases in GHGs. This conclusion is substantiated by very robust climate modelling results, based on a whole hierarchy of models.

The response of the Southern Ocean to ozone depletion is less clear than the atmospheric response. Oceanographic observations are ambiguous with regard to whether or not the Antarctic Circumpolar Current and Southern Ocean overturning have strengthened in recent decades as a result of the poleward intensification of the surface westerly winds. Some strengthening of the ACC/MOC is expected as a consequence of enhanced wind-driven Ekman transport; however, this effect may have been largely offset by increases in mesoscale eddy activity. Determining, precisely, how the Southern Ocean circulation has responded to ozone depletion, and the associated poleward intensification of the westerly winds, is critical because climate models project that the recent wind trends will continue throughout the twenty-first century (albeit with a different seasonality and potentially a different magnitude than were observed in the past). The circulation response to these future changes in the winds will affect the rates of oceanic uptake of heat and anthropogenic carbon, with possible implications for the rate and magnitude of global warming.

The story of Antarctic sea ice is also complicated because the observed sea-ice expansion during the satellite era is inconsistent with expectations based on the positive trend in the SAM.

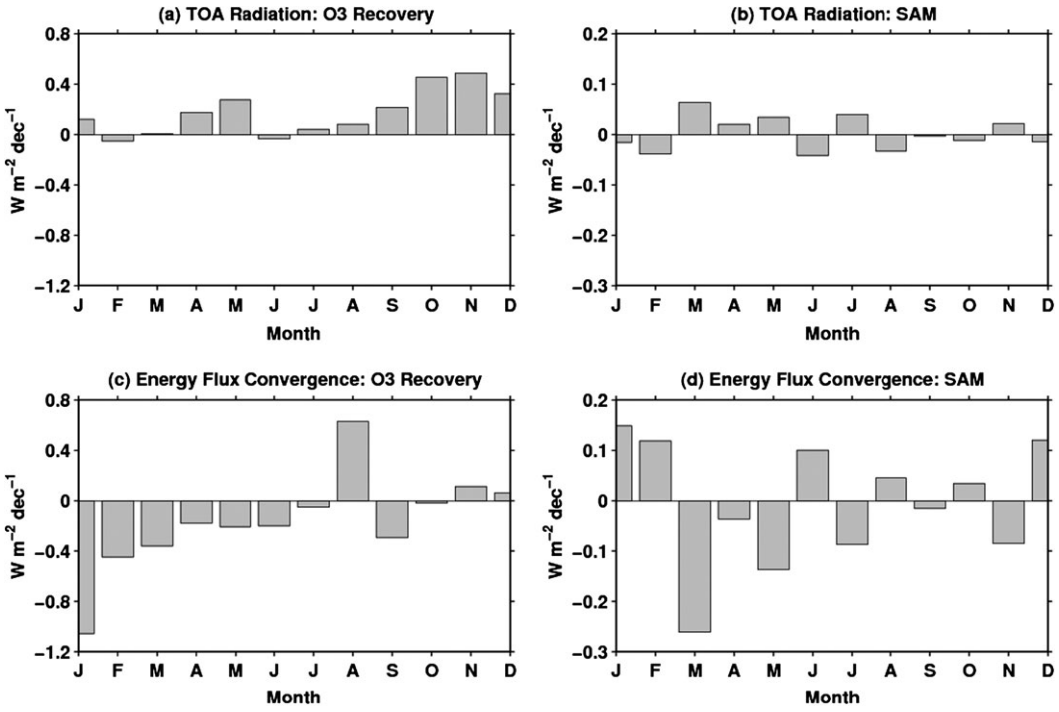

Figure 19. CESM1 simulated linear trends (in W m^{-2} per decade) in the polar-cap (70–90°S) averaged TOA net (SW + LW) incoming radiation ((a) and (b)), and the horizontal convergence of the atmospheric energy transport ((c) and (d)), over the period 2001–2065 (see Smith *et al.*, 2013). The response to stratospheric ozone recovery is shown on the left, while the changes expected based on the SAM trend are plotted on the right.

Although it has been suggested that the sea-ice response to ozone depletion may not be mediated entirely through the SAM (Turner *et al.*, 2009), thus offering the possibility of reconciling the observational data, more recent modelling evidence indicates that ozone depletion acts to decrease Antarctic SIE rather than increase it. It has been argued that the observed sea-ice expansion might not be a response to external forcing, but instead could be a reflection of internal variability within the climate system. However, alternative hypotheses to explain the observed sea-ice changes have also been proposed. For example, Bintanja *et al.* (2013) have suggested that increased meltwater from Antarctic ice shelves has led to a cooling and freshening of the ocean surface layer in recent decades. This could have effectively shielded Antarctic sea ice from the upwelling of warmer water from depth, contributing to the observed increase in SIE. This proposed mechanism has recently been called into question, however (Swart and Fyfe, 2013). Clearly, there is no simple answer when it comes to explaining the observed sea-ice changes. Whatever the answer may be, though, it almost certainly involves ozone depletion at some level.

Finally, the climate impacts of stratospheric ozone depletion are expected to reverse in the coming decades as stratospheric ozone recovery becomes a reality. Ozone recovery will play an important role in the SH climate system because its impacts will largely offset the impacts of increasing GHGs. Although we have focused in section 5 on how this is likely to affect the atmospheric circulation, we emphasize that the competing effects of ozone recovery and GHG increases also will be crucial for understanding other aspects of future climate change. For example, ozone recovery is expected to mitigate a substantial portion of the Antarctic sea-ice loss brought about by increasing GHGs over the next 50 years (Smith *et al.*, 2012). Our ability to anticipate the future climate impacts of ozone recovery, however, is somewhat limited by an incomplete understanding of what has happened in the recent past. To this end, we stress that further work is needed in order to better understand how the climate system responded to ozone depletion in the late twentieth century. In particular, it will be critical to resolve how the Southern Ocean circulation has changed, as this is key to understanding past changes in sea ice, oceanic CO_2 uptake and ice sheet mass balance.

The path forward should be rooted firmly in observational data. This means both acquiring new observations, and finding novel ways to analyze existing data. Additionally, it will be valuable to examine the climate effects of ozone depletion and recovery using models that have not traditionally been employed, such as Earth system models and stand-alone ice-sheet models. This will allow for quantification of the impacts of ozone forcing on Southern Ocean CO_2 uptake and Antarctic ice sheet mass balance. Mass balance changes due to ozone depletion and recovery have yet to be quantified, and this should be set as a high priority for future work. These changes may have important implications for past and future trajectories of global sea-level rise.

Acknowledgement

We thank Karen Smith, Ryan Abernathey and two anonymous reviewers for helpful comments. We also thank Karen Smith for preparing one of the figures. M.P. acknowledges helpful conversations with Kevin Grise. This work was supported by a grant to Columbia University from the National Science Foundation.

References

Abernathey R, Marshall J, Ferreira D. 2011. The dependence of Southern Ocean meridional overturning on wind stress. *J. Phys. Oceanogr.* **41**: 2261–2278.
Arblaster JM, Meehl GA. 2006. Contributions of external forcings to Southern Annular Mode trends. *J. Clim.* **19**: 2896–2905.
Arzel O, Fichefet T, Goosse H. 2006. Sea ice evolution over the 20th and 21st centuries as simulated by current AOGCMs. *Ocean Model.* **12**: 401–415.
Baldwin MP, Dunkerton TJ. 1999. Propagation of the Arctic Oscillation from the stratosphere to the troposphere. *J. Geophys. Res.* **104**: 30937–30946, doi: 10.1029/1999JD900445.
Baldwin MP, Dunkerton TJ. 2001. Stratospheric harbingers of anomalous weather regimes. *Science* **244**: 581–584.
Barnes EA, Barnes NW, Polvani LM. 2014. Delayed Southern Hemisphere climate change induced by stratospheric ozone recovery, as projected by the CMIP5 models. *J. Clim.* **27**: 852–867.

Bi D, Budd WF, Hirst AC, Wu X. 2002. Response of the Antarctic Circumpolar Current transport to global warming in a coupled model. *Geophys. Res. Lett.* **29**: 26–1–26–4, doi: 10.1029/2002GL015919.
Bintanja R, van Oldenborgh GJ, Drijfhout SS, Wouters B, Katsman CA. 2013. Important role for ocean warming and increased ice-shelf melt in Antarctic sea-ice expansion. *Nat. Geosci.* **6**: 376–379.
Bitz CM, Polvani LM. 2012. Antarctic climate response to stratospheric ozone depletion in a fine resolution ocean climate model. *Geophys. Res. Lett.* **39**: L20705, doi: 10.1029/2012GL053393.
Böning CW, Dispert A, Visbeck M, Rintoul SR, Schwarzkopf FU. 2008. The response of the Antarctic Circumpolar Current to recent climate change. *Nat. Geosci.* **1**: 864–869.
Butler AH, Thompson DWJ, Heikes R. 2010. The steady-state atmospheric circulation response to climate change-like thermal forcings in a simple general circulation model. *J. Clim.* **23**: 3474–3496.
Cai W, Cowan T. 2007. Trends in Southern Hemisphere circulation in IPCC AR4 models over 1950–99: Ozone depletion versus greenhouse forcing. *J. Clim.* **20**: 681–693.
Ceppi P, Hwang Y– T, Frierson DMW, Hartmann DL. 2012. Southern Hemisphere jet latitude biases in CMIP5 models linked to shortwave cloud forcing. *Geophys. Res. Lett.* **39**: L19708, doi: 10.1029/2012GL053115.
Cionni I, Eyring V, Lamarque JF, Randel WJ, Stevenson DS, Wu F, Bodeker GE, Shepherd TG, Shindell DT, Waugh DW. 2011. Ozone database in support of CMIP5 simulations: Results and corresponding radiative forcing. *Atmos. Chem. Phys. Discuss.* **11**: 10875–10933.
Dee DP, Uppala SM, Simmons AJ, Berrisford P, Poli P, Kobayashi S, Andrae U, Balmaseda MA, Balsamo G, Bauer P, Bechtold P, Beljaars ACM, van de Berg L, Bidlot J, Bormann N, Delsol C, Dragani R, Fuentes M, Geer AJ, Haimberger L, Healy SB, Hersbach H, Hólm EV, Isaksen L, Kållberg P, Köhler M, Matricardi M, McNally AP, Monge-Sanz BM, Morcrette JJ, Park BK, Peubey C, de Rosnay P, Tavolato C, Thépaut JN, Vitart F. 2011. The ERA-Interim reanalysis: Configuration and performance of the data assimilation system. *Q. J. R. Meteorol. Soc.* **137**: 553–597.
Deser C, Phillips A, Bourdette V, Teng H. 2012. Uncertainty in climate change projections: The role of internal variability. *Clim. Dyn.* **38**: 527–546.
Domack E, Duran D, Leventer A, Ishman S, Doane S, McCallum S, Amblas D, Ring J, Gilbert R, Prentice M. 2005. Stability of the Larsen B ice shelf on the Antarctic Peninsula during the Holocene epoch. *Nature* **436**: 681–685.
Eyring V, Cionni I, Bodeker GE, Charlton-Perez AJ, Kinnison DE, Scinocca JF, Waugh DW, Akiyoshi H, Bekki S, Chipperfield MP, Dameris M, Dhomse S, Frith SM, Garny H, Gettelman A, Kubin A, Langematz U, Mancini E, Marchand M, Nakamura T, Oman LD, Pawson S, Pitari G, Plummer DA, Rozanov E, Shepherd TG, Shibata K, Tian W, Braesicke P, Hardiman SC, Lamarque JF, Morgenstern O, Pyle JA, Smale D, Yamashita Y. 2010. Multi-model assessment of stratospheric ozone return dates and ozone recovery in CCMVal-2 models. *Atmos. Chem. Phys.* **10**: 9451–9472.
Farman JC, Gardiner BG, Shanklin JD. 1985. Large losses of total ozone in Antarctica reveal seasonal ClO_x/NO_x interaction. *Nature* **315**: 207–210.
Fogt RL, Perlwitz J, Monaghan AJ, Bromwich DH, Jones JM, Marshall GJ. 2009. Historical SAM variability. Part II: Twentieth-century variability and trends from reconstructions, observations, and the IPCC AR4 models. *J. Clim.* **22**: 5346–5365.
Forster P, Ramaswamy V, Artaxo P, Berntsen T, Betts R, Fahey DW, Haywood J, Lean J, Lowe DC, Myhre G, Nganga J, Prinn R, Raga G, Schulz M, Van Dorland R. 2007. Changes in atmospheric constituents and in radiative forcing. In *Climate Change 2007: The Physical Science Basis. Contribution of Working Group I to the Fourth Assessment Report of the Intergovernmental Panel on Climate Change*, Solomon S, Qin D, Manning M, Chen Z, Marquis M, Averyt KB, Tignor M, Miller HL. (eds.): 129–234. Cambridge University Press: Cambridge, UK and New York, NY.
Fu Q, Johanson CM, Wallace JM, Reichler T. 2006. Enhanced mid-latitude tropospheric warming in satellite measurements. *Science* **312**: 1179.
Fyfe JC, Saenko OA. 2006. Simulated changes in the extratropical Southern Hemisphere winds and currents. *Geophys. Res. Lett.* **33**: L06701, doi: 10.1029/2005GL025332.
Fyfe JC, Saenko OA, Zickfeld K, Eby M, Weaver AJ. 2007. The role of poleward-intensifying winds on Southern Ocean warming. *J. Clim.* **20**: 5391–5400.
Gerber EP, Polvani LM. 2009. Stratosphere-troposphere coupling in a relatively simple AGCM: The importance of stratospheric variability. *J. Clim.* **22**: 1920–1933.
Gillett NP, Thompson DWJ. 2003. Simulation of recent Southern Hemisphere climate change. *Science* **302**: 273–275.
Gillett NP, Kell TD, Jones PD. 2006. Regional climate impacts of the Southern Annular Mode. *Geophys. Res. Lett.* **33**: L23704, doi: 10.1029/2006GL027721.
Gonzalez PLM, Polvani LM, Seager R, Correa GJP. 2013. Stratospheric ozone depletion: A key driver of recent precipitation trends in South Eastern South America. *Clim. Dyn.*, doi: 10.1007/s00382-013-1777-x.
Grise KM, Thompson DWJ, Forster PM. 2009. On the role of radiative processes in stratosphere–troposphere coupling. *J. Clim.* **22**: 4154–4161.
Grise KM, Polvani LM, Tselioudis G, Wu Y, Zelinka MD. 2013. The ozone hole indirect effect: Cloud-radiative anomalies accompanying the poleward shift of the eddy-driven jet in the Southern Hemisphere. *Geophys. Res. Lett.* **40**: 3688–3692, doi: 10.1002/grl.50675.
Hall A, Visbeck M. 2002. Synchronous variability in the Southern Hemisphere atmosphere, sea ice, and ocean resulting from the annular mode. *J. Clim.* **15**: 3043–3057.
Hallberg R, Gnanadesikan A. 2006. The role of eddies in determining the structure and response of the wind-driven Southern Hemisphere overturning: Results from the Modeling Eddies in the Southern Ocean (MESO) project. *J. Phys. Oceanogr.* **36**: 2232–2252.
Hendon HH, Thompson DWJ, Wheeler MC. 2007. Australian rainfall and surface temperature variations associated with the Southern Hemisphere annular mode. *J. Clim.* **20**: 2452–2467.
Henning CC, Vallis GK. 2005. The effects of mesoscale eddies on the stratification and transport of an ocean with a circumpolar channel. *J. Phys. Oceanogr.* **35**: 880–896.
Hogg AM, Meredith MP, Blundell JR, Wilson C. 2008. Eddy heat flux in the Southern Ocean: Response to variable wind forcing. *J. Clim.* **21**: 608–620.
Hu Y, Fu Q. 2007. Observed poleward expansion of the Hadley circulation since 1979. *Atmos. Chem. Phys.* **7**: 5229–5236.
Johanson CM, Fu Q. 2007. Antarctic atmospheric temperature trend patterns from satellite observations. *Geophys. Res. Lett.* **34**: L12703, doi: 10.1029/2006GL029108.
Kalnay E, Kanamitsu M, Kistler R, Collins W, Deaven D, Gandin L, Iredell M, Saha S, White G, Woollen J, Zhu Y, Chelliah M, Ebisuzaki W, Higgins W, Janowiak J, Mo KC, Ropelewski C, Wang J, Leetmaa A, Reynolds R, Jenne R, Joseph D. 1996. The NCEP/NCAR 40-year reanalysis project. *Bull. Am. Meteorol. Soc.* **77**: 437–471.
Kang SM, Polvani LM, Fyfe JC, Sigmond M. 2011. Impact of polar ozone depletion on subtropical precipitation. *Science* **332**: 951–954.
Karpechko AY, Gillett NP, Marshall GJ, Scaife AA. 2008. Stratospheric influence on circulation changes in the Southern Hemisphere troposphere in coupled climate models. *Geophys. Res. Lett.* **35**: L20806, doi: 10.1029/2008GL035354.
Kushner PJ, Polvani LM. 2004. Stratosphere–troposphere coupling in a relatively simple AGCM: The role of eddies. *J. Clim.* **17**: 629–639.
Lee S, Feldstein SB. 2013. Detecting ozone- and greenhouse gas-driven wind trends with observational data. *Science* **339**: 563–567.
Lefebvre W, Goosse H, Timmermann R, Fichefet T. 2004. Influence of the Southern Annular Mode on the sea ice–ocean system. *J. Geophys. Res.* **109**: C09005, doi: 10.1029/2004JC002403.
Lenton A, Codron F, Bopp L, Metzl N, Cadule P, Tagliabue A, Le Sommer J. 2009. Stratospheric ozone depletion reduces ocean carbon uptake and enhances ocean acidification. *Geophys. Res. Lett.* **36**: L12606, doi: 10.1029/2009GL038227.
Le Quéré C, Rödenbeck C, Buitenhuis ET, Conway TJ, Langenfelds R, Gomez A, Labuschagne C, Ramonet M, Nakazawa T, Metzl N, Gillett N, Heimann M. 2007. Saturation of the Southern Ocean CO_2 sink due to recent climate change. *Science* **316**: 1735–1738.
Liu J, Curry JA, Martinson DG. 2004. Interpretation of recent Antarctic sea ice variability. *Geophys. Res. Lett.* **31**: L02205, doi: 10.1029/2003GL018732.
Lovenduski NS, Gruber N, Doney SC. 2008. Toward a mechanistic understanding of the decadal trends in the Southern Ocean carbon sink. *Global Biogeochem. Cycles* **22**: GB3016, doi: 10.1029/2007GB003139.
Mahlstein I, Gent PR, Solomon S. 2013. Historical Antarctic mean sea ice area, sea ice trends, and winds in CMIP5 simulations. *J. Geophys. Res. Atmos.* **118**: 5105–5110, doi: 10.1002/jgrd.50443.
Maksym T, Stammerjohn S, Ackley S, Massom R. 2012. Antarctic sea ice – a polar opposite? *Oceanography* **25**: 140–151.
McLandress C, Shepherd TG, Scinocca JF, Plummer DA, Sigmond M, Jonsson AI, Reader MC. 2011. Separating the dynamical effects of climate change and ozone depletion. Part II: Southern Hemisphere troposphere. *J. Clim.* **24**: 1850–1868.
Manabe S, Wetherald RT. 1967. Thermal equilibrium of the atmosphere with a given distribution of relative humidity. *J. Atmos. Sci.* **24**: 241–259.
Marshall GJ. 2003. Trends in the Southern Annular Mode from observations and reanalyses. *J. Clim.* **16**: 4134–4143.
Marshall GJ. 2007. Half-century seasonal relationships between the Southern Annular Mode and Antarctic temperatures. *Int. J. Climatol.* **27**: 373–383.
Marshall J, Speer K. 2012. Closure of the meridional overturning circulation through Southern Ocean upwelling. *Nat. Geosci.* **5**: 171–180.
Marshall GJ, Orr A, van Lipzig NPM, King JC. 2006. The impact of a changing Southern Hemisphere Annular Mode on Antarctic Peninsula summer temperatures. *J. Clim.* **19**: 5388–5404.
Meredith MP, Hogg AM. 2006. Circumpolar response of Southern Ocean eddy activity to a change in the Southern Annular Mode. *Geophys. Res. Lett.* **33**: L16608, doi: 10.1029/2006GL026499.
Mikaloff Fletcher SE, Gruber N, Jacobson AR, Doney SC, Dutkiewicz S, Gerber M, Follows M, Joos F, Lindsay K, Menemenlis D, Mouchet A, Muller SA, Sarmiento JL. 2006. Inverse estimates of anthropogenic CO_2 uptake, transport, and storage by the ocean. *Global Biogeochem. Cycles* **20**: GB2002, doi: 10.1029/2005GB002530.
Miller RL, Schmidt GA, Shindell DT. 2006. Forced annular variations in the 20th century Intergovernmental Panel on Climate Change Fourth Assessment Report models. *J. Geophys. Res.* **111**: D18101, doi: 10.1029/2005JD006323.
Min S-K, Son S-W. 2013. Multimodel attribution of the Southern Hemisphere Hadley cell widening: Major role of ozone depletion. *J. Geophys. Res. Atmos.* **118**: 3007–3015.
Molina LT, Molina MJ. 1987. Production of Cl_2O_2 from the self-reaction of the ClO radical. *J. Phys. Chem.* **91**: 433–436.
Monaghan AJ, Bromwich DH, Wang S-H. 2006. Recent trends in Antarctic snow accumulation from Polar MM5 simulations. *Philos. Trans. R. Soc. London, Ser. A* **364**: 1683–1708.
O'Donnell R, Lewis N, McIntyre S, Condon J. 2011. Improved methods for PCA-based reconstructions: Case study using the Steig *et al.* (2009) Antarctic temperature reconstruction. *J. Clim.* **24**: 2099–2115.
Parkinson CL, Cavalieri DJ. 2012. Antarctic sea ice variability and trends, 1979–2010. *Cryosphere* **6**: 871–880.

Polvani LM, Kushner PJ. 2002. Tropospheric response to stratospheric perturbations in a relatively simple general circulation model. *Geophys. Res. Lett.* **29**: 18–1–18–4, doi: 10.1029/2001GL014284.
Polvani LM, Smith KL. 2013. Can natural variability explain observed Antarctic sea ice trends? New modeling evidence from CMIP5. *Geophys. Res. Lett.* **40**: 3195–3199, doi: 10.1002/grl.50578.
Polvani LM, Previdi M, Deser C. 2011a. Large cancellation, due to ozone recovery, of future Southern Hemisphere atmospheric circulation trends. *Geophys. Res. Lett.* **38**: L04707, doi: 10.1029/2011GL046712.
Polvani LM, Waugh DW, Correa GJP, Son S– W. 2011b. Stratospheric ozone depletion: The main driver of twentieth-century atmospheric circulation changes in the Southern Hemisphere. *J. Clim.* **24**: 795–812.
Previdi M, Smith KL, Polvani LM. 2013. The Antarctic atmospheric energy budget. Part I: Climatology and intraseasonal-to-interannual variability. *J. Clim.* **26**: 6406–6418.
Randel WJ, Shine KP, Austin J, Barnett J, Claud C, Gillett NP, Keckhut P, Langematz U, Lin R, Long C, Mears C, Miller A, Nash J, Seidel DJ, Thompson DWJ, Wu F, Yoden S. 2009. An update of observed stratospheric temperature trends. *J. Geophys. Res.* **114**: D02107, doi: 10.1029/2008JD010421.
Rignot E. 1998. Fast recession of a West Antarctic glacier. *Science* **281**: 549–551.
Rignot E. 2011. Is Antarctica melting? *WIREs Clim. Change* **2**: 324–331.
Rignot E, Casassa G, Gogineni P, Krabill W, Rivera A, Thomas R. 2004. Accelerated ice discharge from the Antarctic Peninsula following the collapse of Larsen B ice shelf. *Geophys. Res. Lett.* **31**: L18401, doi: 10.1029/2004GL020697.
Sabine CL, Feely RA, Gruber N, Key RM, Lee K, Bullister JL, Wanninkhof R, Wong CS, Wallace DWR, Tilbrook B, Millero FJ, Peng TH, Kozyr A, Ono T, Rios AF. 2004. The oceanic sink for anthropogenic CO_2. *Science* **305**: 367–371.
Saenko OA, Fyfe JC, England MH. 2005. On the response of the oceanic wind-driven circulation to atmospheric CO_2 increase. *Clim. Dyn.* **25**: 415–426.
Screen JA, Gillett NP, Stevens DP, Marshall GJ, Roscoe HK. 2009. The role of eddies in the Southern Ocean temperature response to the Southern Annular Mode. *J. Clim.* **22**: 806–818.
Sen Gupta A, England MH. 2006. Coupled ocean–atmosphere–ice response to variations in the Southern Annular Mode. *J. Clim.* **19**: 4457–4486.
Sexton DMH. 2001. The effect of stratospheric ozone depletion on the phase of the Antarctic Oscillation. *Geophys. Res. Lett.* **28**: 3697–3700.
Shepherd A, Wingham D, Rignot E. 2004. Warm ocean is eroding West Antarctic ice sheet. *Geophys. Res. Lett.* **31**: L23402, doi: 10.1029/2004GL021106.
Shindell DT, Schmidt GA. 2004. Southern Hemisphere climate response to ozone changes and greenhouse gas increases. *Geophys. Res. Lett.* **31**: L18209, doi: 10.1029/2004GL020724.
Sigmond M, Fyfe JC. 2010. Has the ozone hole contributed to increased Antarctic sea ice extent? *Geophys. Res. Lett.* **37**: L18502, doi: 10.1029/2010GL044301.
Sigmond M, Fyfe JC, Scinocca JF. 2010. Does the ocean impact the atmospheric response to stratospheric ozone depletion? *Geophys. Res. Lett.* **37**: L12706, doi: 10.1029/2010GL043773.
Sigmond M, Reader MC, Fyfe JC, Gillett NP. 2011. Drivers of past and future Southern Ocean change: Stratospheric ozone versus greenhouse gas impacts. *Geophys. Res. Lett.* **38**: L12601, doi: 10.1029/2011GL047120.
Simmonds I, Keay K. 2000. Variability of Southern Hemisphere extratropical cyclone behavior, 1958–97. *J. Clim.* **13**: 550–561.
Simpkins GR, Ciastro LM, Thompson DWJ, England MH. 2012. Seasonal relationships between large-scale climate variability and Antarctic sea ice concentration. *J. Clim.* **25**: 5451–5469.
Smith KL, Polvani LM, Marsh DR. 2012. Mitigation of 21st century Antarctic sea ice loss by stratospheric ozone recovery. *Geophys. Res. Lett.* **39**: L20701, doi: 10.1029/2012GL053325.
Smith KL, Previdi M, Polvani LM. 2013. The Antarctic atmospheric energy budget. Part II: The effect of ozone depletion and its projected recovery. *J. Clim.* **26**: 9729–9744.
Solomon S. 1999. Stratospheric ozone depletion: A review of concepts and history. *Rev. Geophys.* **37**: 275–316.
Solomon S, Garcia RR, Rowland FS, Wuebbles DJ. 1986. On the depletion of Antarctic ozone. *Nature* **321**: 755–758.
Son S-W, Tandon NF, Polvani LM, Waugh DW. 2009. Ozone hole and Southern Hemisphere climate change. *Geophys. Res. Lett.* **36**: L15705, doi: 10.1029/2009GL038671.
Son S-W, Gerber EP, Perlwitz J, Polvani LM, Gillett NP, Seo K-H, Eyring V, Shepherd TG, Waugh D, Akiyoshi H, Austin J, Baumgaertner A, Bekki S, Braesicke P, Brühl C, Butchart N, Chipperfield MP, Cugnet D, Dameris M, Dhomse S, Frith S, Garny H, Garcia R, Hardiman SC, Jöckel P, Lamarque JF, Mancini E, Marchand M, Michou M, Nakamura T, Morgenstern O, Pitari G, Plummer DA, Pyle J, Rozanov E, Scinocca JF, Shibata K, Smale D, Teyssèdre H, Tian W, Yamashita Y. 2010. Impact of stratospheric ozone on Southern Hemisphere circulation change: A multimodel assessment. *J. Geophys. Res.* **115**: D00M07, doi: 10.1029/2010JD014271.
Steig EJ, Schneider DP, Rutherford SD, Mann ME, Comiso JC, Shindell DT. 2009. Warming of the Antarctic ice-sheet surface since the 1957 International Geophysical Year. *Nature* **457**: 459–463.
Swart NC, Fyfe JC. 2012. Observed and simulated changes in the Southern Hemisphere surface westerly wind-stress. *Geophys. Res. Lett.* **39**: L16711, doi: 10.1029/2012GL052810.
Swart NC, Fyfe JC. 2013. The influence of recent Antarctic ice sheet retreat on simulated sea ice area trends. *Geophys. Res. Lett.* **40**: 4328–4332, doi: 10.1002/grl.50820.
Tedesco M, Monaghan AJ. 2009. An updated Antarctic melt record through 2009 and its linkages to high-latitude and tropical climate variability. *Geophys. Res. Lett.* **36**: L18502, doi: 10.1029/2009GL039186.
Thomas R, Rignot E, Casassa G, Kanagaratnam P, Acuña C, Akins T, Brecher H, Frederick E, Gogineni P, Krabill W, Manizade S, Ramamoorthy H, Rivera A, Russell R, Sonntag J, Swift R, Yungel J, Zwally J. 2004. Accelerated sea-level rise from West Antarctica. *Science* **306**: 255–258.
Thomas ER, Marshall GJ, McConnell JR. 2008. A doubling in snow accumulation in the western Antarctic Peninsula since 1850. *Geophys. Res. Lett.* **35**: L01706, doi: 10.1029/2007GL032529.
Thompson DWJ, Solomon S. 2002. Interpretation of recent Southern Hemisphere climate change. *Science* **296**: 895–899.
Thompson DWJ, Wallace JM. 2000. Annular modes in the extratropical circulation. Part I: Month-to-month variability. *J. Clim.* **13**: 1000–1016.
Thompson DWJ, Lee S, Baldwin MP. 2003. Atmospheric processes governing the Northern Hemisphere Annular Mode/North Atlantic Oscillation. In *The North Atlantic Oscillation: Climatic Significance and Environmental Impact*, Hurrell JW, Kushnir Y, Ottersen G, Visbeck G. (eds.) *AGU Geophysical Monograph* 134: 81–112 American Geophysical Union: Washington, DC.
Thompson DWJ, Baldwin MP, Solomon S. 2005. Stratosphere–troposphere coupling in the Southern Hemisphere. *J. Atmos. Sci.* **62**: 708–715.
Thompson DWJ, Solomon S, Kushner PJ, England MH, Grise KM, Karoly DJ. 2011. Signatures of the Antarctic ozone hole in Southern Hemisphere surface climate change. *Nat. Geosci.* **4**: 741–749.
Treguier AM, Le Sommer J, Molines JM, de Cuevas B. 2010. Response of the Southern Ocean to the Southern Annular Mode: Interannual variability and multidecadal trend. *J. Phys. Oceanogr.* **40**: 1659–1668.
Turner J, Comiso JC, Marshall GJ, Lachlan-Cope TA, Bracegirdle T, Maksym T, Meredith MP, Wang Z, Orr A. 2009. Non-annular atmospheric circulation change induced by stratospheric ozone depletion and its role in the recent increase of Antarctic sea ice extent. *Geophys. Res. Lett.* **36**: L08502, doi: 10.1029/2009GL037524.
Turner J, Bracegirdle T, Phillips T, Marshall GJ, Hosking JS. 2013. An initial assessment of Antarctic sea ice extent in the CMIP5 models. *J. Clim.* **26**: 1473–1484.
Ummenhofer CC, Sen Gupta A, England MH. 2009. Causes of late twentieth-century trends in New Zealand precipitation. *J. Clim.* **22**: 3–19.
Van den Broeke M, van Lipzig NPM. 2004. Changes in Antarctic temperature, wind and precipitation in response to the Antarctic Oscillation. *Ann. Glaciol.* **39**: 119–126.
Van den Broeke M, van de Berg W, van Meijgaard E. 2006. Snowfall in coastal West Antarctica much greater than previously assumed. *Geophys. Res. Lett.* **33**: L02505, doi: 10.1029/2005GL025239.
Wang XL, Feng Y, Compo GP, Swail VR, Zwiers FW, Allan RJ, Sardeshmukh PD. 2013. Trends and low frequency variability of extra-tropical cyclone activity in the ensemble of twentieth century reanalysis. *Clim. Dyn.* **40**: 2775–2800.
Waugh DW, Randel WJ, Pawson S, Newman PA, Nash ER. 1999. Persistence of the lower stratospheric polar vortices. *J. Geophys. Res.* **104**: 27191–27201, doi: 10.1029/1999JD900795.
Waugh DW, Primeau F, DeVries T, Holzer M. 2013. Recent changes in the ventilation of the southern oceans. *Science* **339**: 568–570.
World Meteorological Organization (WMO). 2011. 'Scientific assessment of ozone depletion: 2010', Global Ozone Research and Monitoring Project Report No. 52. WMO: Geneva, Switzerland.
Young PJ, Butler AH, Calvo N, Haimberger L, Kushner PJ, Marsh DR, Randel WJ, Rosenlof KH. 2013. Agreement in late twentieth century Southern Hemisphere stratospheric temperature trends in observations and CCMVal-2, CMIP3, and CMIP5 models. *J. Geophys. Res. Atmos.* **118**: 605–613, doi: 10.1002/jgrd.50126.
Zelinka MD, Klein SA, Hartmann DL. 2012. Computing and partitioning cloud feedbacks using cloud property histograms. Part I: Cloud radiative kernels. *J. Clim.* **25**: 3715–3735.
Zunz V, Goosse H, Massonnet F. 2013. How does internal variability influence the ability of CMIP5 models to reproduce the recent trend in Southern Ocean sea ice extent? *Cryosphere* **7**: 451–468.

